# PHOTOPHYSICS OF QUANTUM EMITTERS IN HEXAGONAL BORON NITRIDE

A THESIS SUBMITTED TO
THE GRADUATE SCHOOL OF ENGINEERING AND SCIENCE
OF BILKENT UNIVERSITY
IN PARTIAL FULFILLMENT OF THE REQUIREMENTS FOR
THE DEGREE OF
MASTER OF SCIENCE
IN
MATERIALS SCIENCE AND NANOTECHNOLOGY

By
Hilal Korkut
September 2022

PHOTOPHYSICS OF QUANTUM EMITTERS IN HEXAGONAL BORON NITRIDE
By Hilal Korkut
September 2022

We certify that we have read this thesis and that in our opinion it is fully adequate, in scope and in quality, as a thesis for the degree of Master of Science.

İbrahim Sarpkaya(Advisor)

Bülend Ortaç

Serkan Ateş

Approved for the Graduate School of Engineering and Science:

Orhan Arıkan
Director of the Graduate School

# ABSTRACT

# PHOTOPHYSICS OF QUANTUM EMITTERS IN HEXAGONAL BORON NITRIDE

Hilal Korkut
M.S. in Materials Science and Nanotechnology
Advisor: İbrahim Sarpkaya
September 2022

Since the discovery of graphene in 2004, two-dimensional (2D) materials have attracted a great deal of attention. Due to its distinct optical, mechanical, and electrical properties, hexagonal boron nitride (h-BN) has been considered for both fundamental research and device applications. The recent observation of room temperature single photon emission from h-BN defect centers makes it also exciting material platform for applications of quantum photonics. Single-photon sources play an essential role in quantum technologies such as quantum computing, quantum sensing, and quantum telecommunication. These quantum technologies correspond to quantum physics and utilize features namely, interference, superposition, entanglement, and squeezed states. Therefore, require bright, indistinguishable, and pure single-photons. Quantum emitters in h-BN have been investigated extensively in recent years due to their high brightness, high stability, and spectral tunability. Although the exact microscopic origin of quantum emitters is unknown, it is attributed to deep-defect emission because of the presence of defect centers in h-BN. In order to study the photophysics of quantum emitters in h-BN, we have utilized thermal annealing processes to create optically active defect centers on commercially available solution-based h-BN flakes. First, we performed optical characterizations at room temperature to see whether we created defect centers successfully or not. Then, to investigate the photostability of emitters, we performed photoluminescence (PL) and spectral diffusion measurements at liquid helium temperature. After confirming the photostability of those PL emissions, we performed photon antibunching measurements by using Hanbury Brown and Twiss interferometer in order to investigate the quantum nature of those PL emissions.

By using the time-correlated single-photon counting method, we have also measured the lifetimes of those quantum emitters. Finally, we performed magneto-PL measurements and studied spin defects under an applied out-of-plane magnetic field. A substantial decrease in the integrated PL intensity of the emitters by up to one order of magnitude was observed when the applied field is increased from 0T to 7T. The observed photodarkening in the PL emission intensity of the quantum emitters has been attributed to the presence of spin-selective, nonradiative intersystem crossing (ISC) transitions.

*Keywords:* Hexahonal boron nitride, quantum emitter, thermal anneling, spin defect.

# ÖZET

# ALTIGEN BOR NİTRÜRDEKİ KUANTUM YAYICILARIN FOTOFİZİĞİ

Hilal Korkut
Malzeme Bilimi ve Nanoteknoloji, Yüksek Lisans
Tez Danışmanı: İbrahim Sarpkaya
Eylül 2022

2004 yılında grafenin keşfinden bu yana, iki boyutlu (2D) malzemeler büyük ilgi gördü. Farklı optik, mekanik ve elektriksel özelliklerinden dolayı altıgen bor nitrür (h-BN) hem temel araştırma hem de cihaz uygulamaları için düşünülmüştür. h-BN kusur merkezlerinden oda sıcaklığındaki tek foton emisyonunun yakın zamanda gözlemlenmesi, onu kuantum fotonik uygulamaları için de heyecan verici bir malzeme platformu haline getiriyor. Tek foton kaynakları, kuantum hesaplama, kuantum algılama ve kuantum telekomünikasyon gibi kuantum teknolojilerinde önemli bir rol oynar. Bu kuantum teknolojileri, kuantum fiziğine karşılık gelir ve girişim, süperpozisyon, dolaşma ve sıkıştırılmış durumlar gibi özellikler kullanır. Bu nedenle, parlak, ayırt edilemez ve saf tek fotonlar gerektirir. h-BN'deki kuantum yayıcılar, yüksek parlaklıkları, yüksek kararlılıkları ve spektral ayarlanabilirlikleri nedeniyle son yıllarda kapsamlı bir şekilde araştırılmıştır. Kuantum yayıcıların tam mikroskobik kökeni bilinmemekle birlikte, h-BN'deki kusur merkezlerinin varlığından dolayı derin kusur emisyonuna atfedilir. h-BN'deki kuantum yayıcıların fotofiziğini incelemek için, ticari olarak temin edilebilen çözelti bazlı h-BN pulları üzerinde optik olarak aktif kusur merkezleri oluşturmak için termal tavlama işlemlerini kullandık. İlk olarak, hata merkezlerini başarılı bir şekilde oluşturup oluşturmadığımızı görmek için oda sıcaklığında optik karakterizasyonlar yaptık. Ardından emitörlerin fotostabilitesini araştırmak için sıvı helyum sıcaklığında fotolüminesans (PL) ve spektral difüzyon ölçümleri yaptık. Bu PL emisyonlarının fotostabilitesini onayladıktan sonra, bu PL emisyonlarının kuantum yapısını araştırmak için Hanbury Brown ve Twiss interferometre kullanarak foton antibunching ölçümleri gerçekleştirdik. Zamana bağlı tek foton sayma yöntemini kullanarak, bu kuantum yayıcıların ömürlerini de ölçtük. Son olarak, manyeto-PL ölçümleri yaptık ve uygulanan düzlem dışı manyetik alan altında spin kusurlarını inceledik. Uygulanan alan

0T'den 7T'ye yükseltildiğinde, yayıcıların entegre PL yoğunluğunda bir büyüklük sırasına kadar önemli bir azalma gözlemlendi. Kuantum yayıcıların PL emisyon yoğunluğunda gözlenen fotokarartma, dönüş seçici, ışınımsal olmayan sistemler arası geçiş (ISC) geçişlerinin varlığına bağlanmıştır.

*Anahtar sözcükler*: Altıgen bor nitrür, kuantum yayıcı, termal tavlama, spin kusurları.

# Acknowledgement

Foremost, I would like to sincerely thank my advisor Assist. Prof. İbrahim Sarpkaya for his guidance, and support throughout my master's study. His guidance, enthusiasm, motivation, and faith in me helped me a lot during the research.

Besides, I would like to thank my thesis committee: Assist. Prof. Bülend Ortaç and Associate Prof. Serkan Ateş, for their comments and questions. I thank Assist. Prof. Talip Serkan Kasırga and his group members for being patient and kind time to me. Throughout my research, I used their laboratory and equipment. Whenever I needed they helped me.

I want to acknowledge support from Bilkent University, TUBİTAK-BİDEB 2232 International Fellowship for Outstanding Researcher Program, and UNAM for providing financial support for this work.

I would like to thank all the talented engineers of Bilkent University, UNAM for their patience and kindness, and help. I thank my fellow lab mates in Quantum Photonics Group: Mehmet Atıf Durmuş, Şeyma Esra Atalay, Ali Hakim Taşkıran, Salih Işıksaçan and Kaan Demiralay. I had so much fun with you in Unam

Also, I thank my friends Gözde Tuman and Senem Kaylar for their wonderful friendship and their faith in me, and for being there for me in difficult times.

Last but not least, I would like to thank my family: my parents Cemile and Ahmet Korkut, and my brother Tunahan for always supporting and being there for me throughout my life. I would not be able to be here today if weren't for you.

# Contents

# List of Figures

# List of Tables

# Chapter 1

# Introduction

Since the antibunched light was first observed by Kimble et al. in 1977, solid-state single-photon emitters have been playing an essential role in quantum technologies [1] such as quantum computing, [2] quantum imaging, [3] quantum sensing, [4] and quantum internet [5].Hexagonal boron nitride is one of the promising candidates that hosts quantum emitters.We studied the photophysical properties of quantum emitters in hexagonal boron nitride (h-BN). Quantum technologies correspond to quantum physics and utilize features including entanglement, interference, superposition, and squeezed states [6, 7, 8]. Classical computers employ binary systems, which can be either 0s or 1s. Quantum computers use quantum bits or qubits, a qubit can be either 0 or 1 or can be a superposition of 0 and 1. A group of qubits can be in any superposition. This considerably enhances the type of information that may be represented and makes it possible to take advantage of quantum interference.[9] Compared to classical computers, quantum algorithms can solve complex problems much faster. Classical encryption has been severely constrained by the large integer factorization problem, however, quantum computers can overcome this barrier by using Shor's algorithm. [10, 11] The ability to sense phase, magnetic field, and polarization is improved by the squeezed states of light. Squeezed states of light can reduce measurement uncertainty.

New prospects for precision sensing in science have been made possible by quantum sensors that utilize squeezed state of light. [12, 13] Another quantum application is quantum key distribution (QKD). It is an application that, despite the eavesdroppers, allows secure communication and distributes quantum bits in accordance with the laws of physics. Various QKD protocols have been developed over time, and experimental studied have been carried out. [14]

Numerous methods and materials have been investigated over time to produce single photons. There are several promising solid-state single-photon emitters, including quantum dots, [15] carbon nanotubes, [16] colour centers in diamond, [17] and two dimensional layered materials such as transition metal dichalcogenides (TMDs) [18] and hexagonal boron nitride [19]. Brightness, purity, indistinguishability, and stability are the characteristics of the ideal single-photon source. [20]Depending on the single-photon source operating temperature, emission wavelength, advantages, and disadvantages vary. [21] Colour centers in diamond operate at room temperature, quantum emitters show photostability and give emissions around 640-800 nm. [22, 23] There are several requirements for quantum network applications. For instance, the ability to successfully interface qubits with photons in order to achieve remote entanglement, the capacity to store quantum states while entanglement is being generated, and the capacity to operate with high fidelity and store several entanglement states. The majority of these requirements are met by color centers in diamonds, thus potential candidates for the quantum network application. [24] With high single-photon purity and emission at the telecom wavelength ranges of O-band and C-band, quantum dots are excellent candidates for quantum telecommunication applications. They do, however, operate at cryogenic temperature. [25, 26, 27] Studies have showed that carbon nanotubes emit photon at a long wavelength range between 1000-1500 µm but suffer from low brightness. [28, 29] Two dimensional layered materials (TMDs) exhibits extraordinary mechanical, electrical, and optical properties compare to bulks. Due to the atomic thicknesses, these properties can be modified by doping and strain. [30] Bandgap of TMDs transform from indirect to direct when thickness is reduced from bulk to monolayer.

Single-photon generation can be achieved either by monolayer TMDs (MoS2, WSe2) or heterostructure of TMDs (WSe2/MoSe2). MoS2, WSe2, MoSe2, and WS2 are particularly fascinating since they have a visible region direct bandgap. For light emitting diodes, laser, and photodetectors TMDs are used. [31, 32, 33]

In recent years two-dimensional van der Waals hexagonal boron nitride have become attractive due to its unique chemical, optical, electronic, and mechanical properties. [34, 35] Single photon emission wavelength spectra vary from ultraviolet (UV) to near-infrared, [36] and can be modified by applied electric field or strain. [37] Therefore, it has attracted the attention of researchers for quantum photonics applications.37 The exceptional properties of quantum emitters in h-BN such as high brightness at room temperature, [38] high thermal stability up to 1100 K, [39] and large Debye-Waller factor [40] make them prominent in quantum photonics applications. Recent studies have also shown spin defects in h-BN by carrying out optically detected magnetic resonance (ODMR) measurements as well as magneto-PL measurements. [41, 42] For quantum networks and quantum sensing applications, spin defect centers are very significant. [43, 44] Even though the origin of single-photon emission in h-BN is under debate, it is attributed to deep-defect level emissions due to the defect centers in h-BN such as vacancy-related, and substitutional defect centers. [20, 45] There are different post processes are used to create optically active defect centers such as thermal annealing, electron irradiation, and ion implantation. [46, 47, 48] Here, we studied photoluminescence (PL) emission dynamics of quantum emitters in h-BN by performing various experiments. To determine whether we created an optically active defect center or not, we first carried out optical characterizations at room temperature using the photoluminescence spectroscopy technique. After confirming and finding the different PL emissions at various wavelengths in the visible range, we performed PL emission and spectral diffusion measurements at low temperature (3.5 K) by using a home-built micro-PL setup. Furthermore, to study the photophysics of quantum emitters in h-BN, we also carried out lifetime measurements.

Using Hanbury Brown and Twiss interferometer, we performed antibunching measurements to study the quantum nature of emitters in h-BN. Finally, confirming stable PL emissions that show quantum nature, we studied the PL emissions dynamics of quantum emitters in h-BN under an applied out-of-plane external magnetic field at cryogenic temperature. We observed photodarkening of PL emissions under applied magnetic field if the spin-dependent non-radiative intersystem crossing (ISC) transitions occur.

# Chapter 2

# Theoretical Basis

Quantum photonics is a study field that investigates the quanta of light (photon) and matter interaction and understanding of the nature of the photons. [49] The word "photon" is produced from Greek. Photo means light in Greek and later the "-on" was started to use at the end. In today's literature "photonics" is used almost the same sense as "optics". [50] Our understanding of light has changed and diverse theories have been developed over the years. The theory of quantum light is comprehensive and explains practically whole optical phenomena. [51] There are several underlying developments before the quantum photonic model was introduced. In the early progress, there were two theories one was particle theory suggested by Newton and the other was wave theory explained by Huygens. The wave theory of light was justified via Young's double-slit experiment in 1801. Later, with the derivation of Maxwell's famous equations, the electromagnetic wave model of light was presented.In the early twentieth century, physicists struggled to explain black-body radiation due to the discrepancy between theoretical expectations and experimental results called the ultraviolet catastrophe problem. In 1901, to fulfill the experimental data Planck suggested that black-body radiation only can be emitted or absorbed as discrete energy ($E = nh\nu$, n= 1,2,3,. . . , and h=6,62607004 x 10-34 $m^2$ kg / s) packets. In 1905, Einstein adopted Plank's theory and defined the photoelectric effect. [50, 52]

The first trial of the quantum optic experiment was carried out to illustrate the interference of light by Taylor in 1909. He used Young's double-slit experiment and sent low-intensity light through the slits. [53] The quantum theory of light emerged after quantum mechanics was born in 1924. Later Paul Dirac published his paper called "the quantum theory of the emission and the absorption of radiation" in 1927. [54] The contemporary quantum photonics model was built after an interference experiment by Hanbury Brown and Twiss in 1956. Their experimental finding could be clarified only by referring to quantum theory. [52]

## 2.1 Photon Properties

A quantum of light is named a photon. A photon has wave-particle duality. a photon is identified by its energy ($E = h\nu$). Due to the wave duality, a photon has a wavelength, and the wavelength of the photon can alter depending on the refractive index of the medium that it travels through, however, the frequency will remain the same. Contrary to electrons, photons do not interact with each other. Therefore, they cannot interchange energy.

| | Particle | Wave |
|---|---|---|
| Reflection | ✓ | ✓ |
| Refraction | ✓ | ✓ |
| Interference | x | ✓ |
| Diffraction | x | ✓ |
| Polarization | x | ✓ |
| Photoelectric effect | ✓ | x |

Table 2.1: Optical phenomena that indicate wave-particle like the behavior of the photons

A photon mass is equal to zero and its energy is proportional to frequency. Photons are bosons, and they correspond to Bose-Einstein statistics. They can occupy the same space, unlike fermions. Therefore, they are indistinguishable which makes them attractive to quantum technologies. It is possible to restate the wave function of a single photon by sending it to an optical instrument such as a beam splitter.

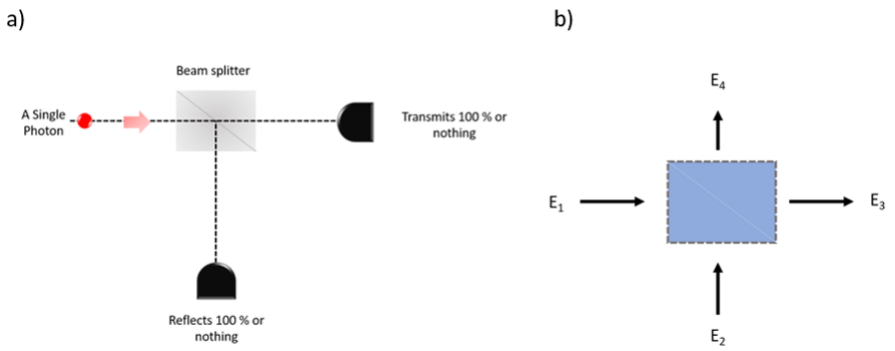


Figure 2.1: Simple model of a) separation b) combination of two photons

When we send the single photon to the beam splitter photon either is going to be transmitted 100 % or reflected, which is used in Hanbury Brown and Twiss interferometer. Moreover, two photons can be consolidated via a beam splitter to study interference fringes. The figure 2.1 shows a basic illustration of restating photons and merging two separate photons. These two phenomena are used in quantum applications. Photons can be emitted or absorbed via energy conservation in materials. [55]The light propagates as photons and a photon can act as a wave and particle. The first person who approached this issue was Isaac Newton. According to him, light travels as small particles. On the other hand, Thomas Young said the light is a wave. Several optical phenomena indicate particle behavior and/or wave behavior.

## 2.2 Radiative Transition in Atoms

Photons can be created (emission) via an optical process called radiative transition. A photon creation can achieve by spontaneous emission or stimulated emission. As we know there are discrete energy levels and sublevels in atomic structure, hence there are different possible transition routes. Therefore, the features of the emitted photons can change depending on the transition route in atomic structure.[56]

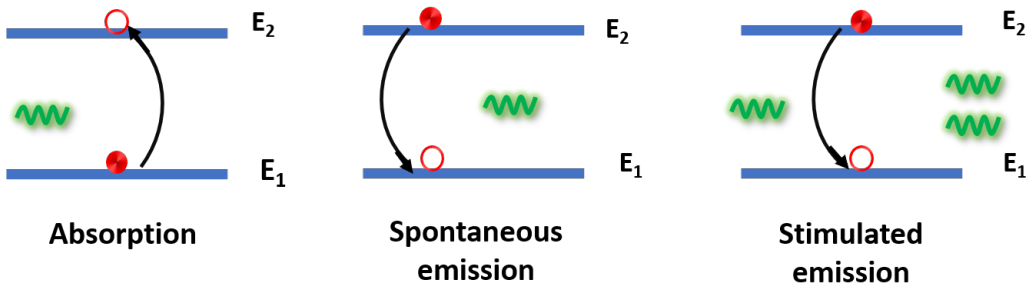


Figure 2.2: The schematic illustration of absorption, spontaneous emission, and stimulated emission

A photon absorption and emission in a two-level quantum system are shown in the figure 2.2. When we excite atomic structure, an electron jumps from a lower state to an upper state, absorption. The required amount of energy to make this jump is equal to $E_2 - E_1$. However, to their nature electrons tend to go back to the initial state or one of the lower states, when they do they give their extra energy as a photon, spontaneous emission. If we excite a quantum system that has already excited two-photon, stimulated emission. The emitted photon is identical to the excitation photon. Stimulated emission was first introduced by Einstein.[57]

## 2.3 Selection rules

There are four quantum numbers to define an electron in the atom.

- Principle quantum number (n)
- Angular quantum number (l)
- Magnetic quantum number (m)
- Spin quantum number (s)

For dipole transitions, there are restrictions on some of the quantum numbers. The angular quantum number l changes between the initial and final state:

$$\Delta \mathrm{l} = \pm 1 \tag{2.1}$$

Photons can be circularly polarized ($\sigma+$ and $\sigma-$) or linearly polarized along the z-axis, y-axis, or x-axis. M number changes vary depending on the light polarization.[52]

- $\Delta_m = +1$ , circularly polarized +
- $\Delta_m = -\ 1$ , circularly polarized -
- $\Delta_m = 0$ , linearly polarized along z-axis
- $\Delta_m = \ \pm 1 \quad$ , linearly polarized along x,y-axis

An electron spin number can be either 1/2 or – 1/ 2. Electrons are fermions, hence corresponding Pauli exclusion principle. Therefore, the spin number changes.

$$\Delta \mathrm{s} = 0 \tag{2.2}$$

Selection rules also apply for quantum systems that have multiple electrons. Quantum numbers for multi-electron quantum systems are L, J, S. Total angular momentum for atom J and number changes

$$\Delta \mathrm{J} = 0, \pm 1 \tag{2.3}$$

however, $0 \rightarrow 0$ is not allowed. Total orbital angular momentum number L changes

$$\Delta \mathrm{L} = 0 \pm 1 \tag{2.4}$$

again, $0 \rightarrow 0$ is not allowed. Total spin number S changes

$$\Delta \mathrm{s} = 0 \tag{2.5}$$

If the quantum number changes satisfy the above equations transitions will be allowed, if not transitions will be forbidden.[57]

## 2.4 Photon statistics

Now we need to understand the characteristic behavior of the light if the photons are created by spontaneous emission or stimulated emission. To do that, first, we need to detect the photons. Emitted photons can be detected via a photon detector. As we know, light-matter interacts in different ways, and a photon detector is a device that produces a current or voltage signal as a result of this interaction.[58] There are different types of lights, namely thermal light, coherent light, and non-classical light. However, this interaction does not give us information about the characteristic behavior of the photons and whether photons are emitted via spontaneous or stimulated emission.[49] Therefore, we need to study photon statistics called Poissonian,[59] Sub-Poissonian,[60] , and Super-Poissonian statistics.[61] Figure 2.3 shows a basic demonstration of how the amplitude of the electric field changes through time. When we look at the fluctuation in the light field we can learn about light behavior. For example, for thermal (chaotic) light, large fluctuations can be observed, and photon detection is much more possible for the higher intensity.[49] Coherent (laser) light emission corresponds to Poissonian statistics.[62] Non-classical light behavior can be understood by studying Sub-Poissonian statistics.[63]

Studying the number of photons detected per unit of time will show us there are different statistics and different probability distributions for different lights. If we look at figure 2.4 we will see the various photon distributions. Photon distribution for coherent (laser) light demonstrates Poissonian statistics, and thermal light states illustrate exponential decay which is a typical Bose-Einstein distribution. The non-classical light distribution shows squeezed or displaced squeezed states.[49]

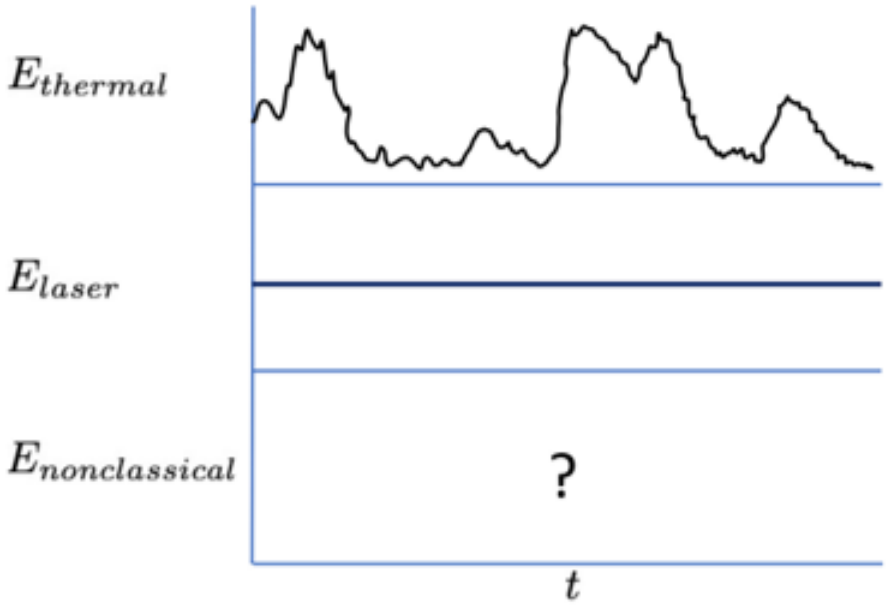


Figure 2.3: Time evolution of the electric field for the different light sources, namely thermal, laser (coherent), and non-classical light. [taken from An Introduction to Quantum Optic by Perry Rice]

Photon counting is a process in which photons are counted via photon detectors. This technique involves a photon detector which can be a photomultiplier tube (PMT) detector[64], avalanche photodiode (APD) detector[65], and counter. When the light beams strike the detector, it produces voltage pulses. The counter connected to the detector counts the number of pulses per unit time and determines the count rate. However, fluctuation in the count rate can be observed from one measurement to another. The fluctuation can be caused by photon statistics or can be an effect of the detection process. We must be careful while differentiating fluctuation due to the nature of the photon detection process or photon statistics of the incident light beam.[52] Therefore, to understand the nature of light, we need to study the degree of optical coherence at two points.[63]

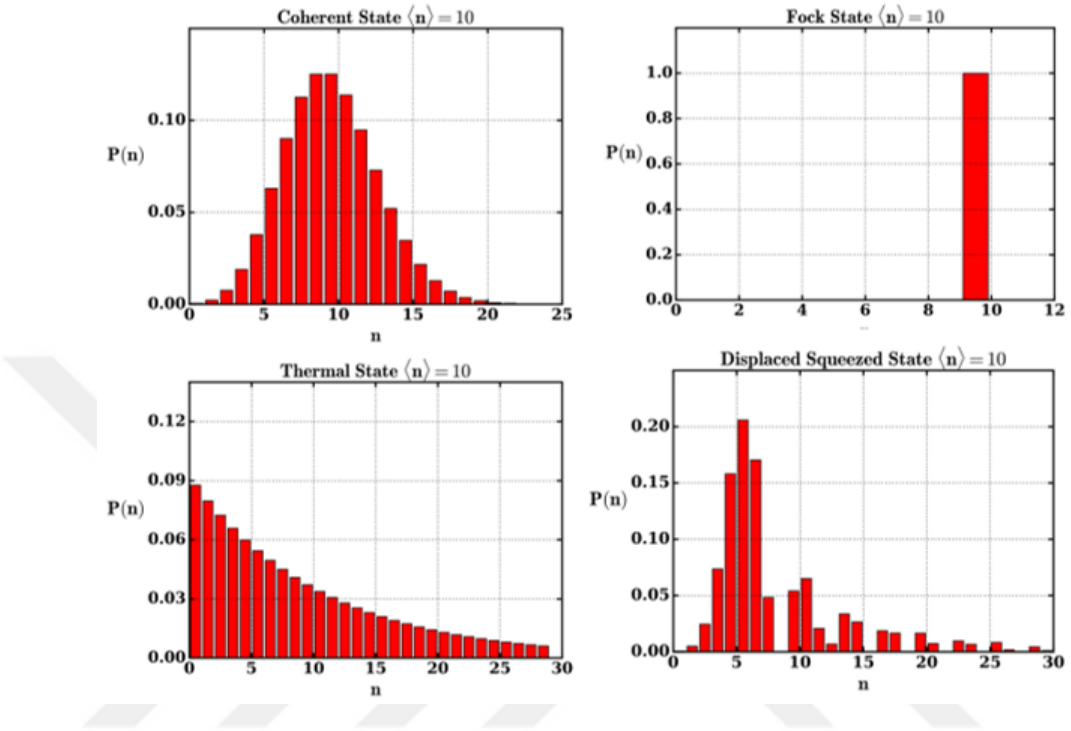


Figure 2.4: Probability distribution of photons for different lights.[taken from An Introduction to Quantum Optic by Perry Rice]

We can classify light according to photon distribution statistics. [52]

| Photon statistics | Type of light | Variance-Mean number |
|---|---|---|
| Super-Poissonian | Thermal | $\Delta n > \sqrt{\bar{n}}$ |
| Poissonian | Cohorent | $\Delta n = \sqrt{\bar{n}}$ |
| Sub-Poissonian | Non-classical | $\Delta n < \sqrt{\bar{n}}$ |

Table 2.2: Classification of the light depending on the photon statistics

## 2.5 Photon Antibunching

While Poissonian and super-Poissonian statistics indicate classical behavior, sub-Poissonian statistics show non-classical light behavior. Another way of determining the nature of the light is by studying the second-order correlation function g2($\tau$). Studying correlation functions allow us to classify light as antibunched, bunched [66] , or coherent.[67] The quantity of the electromagnetic field determines the optical coherence. To understand the nature of the coherent, thermal, and non-classical light first-order and second-order correlation functions are calculated. The interference fringes that are observed in Young's double-slit experiments give us the first-order correlation function. The second-order correlation function can be obtained by the Hanbury Brown-Twiss interferometer which shows the correlation of the light intensity.[68, 63] Only the second-order function can explain the quantum nature of light.

### 2.5.1 The second-order correlation function

As we discussed, the quantum nature of the light can be only explained second-order correlation function. We can write the function as:

$$g^{(2)}(\tau) = \frac{\langle E^*(t)\, E^*(t+\tau)\, E(t+\tau)\, E(t)\rangle}{\langle E^*(t)\, E(t)\rangle \langle E^*(t+\tau)\, E(t+\tau)\rangle} = \frac{\langle I(t)\, I(t+\tau)\rangle}{\langle I(t)\rangle \langle I(t+\tau)\rangle} \tag{2.6}$$

Where E is electric field and I is the intensity of the light. We think average intensity of the light source is constant, $\langle I(t)\rangle = \langle I(t+\tau)\rangle$ and spatially coherent. Under these conditions the second-order correlation function study the temporal coherence the light beam. Now we study the second-order correlation function for different conditions. Coherence time $\tau_c$ of the light source defines the intensity fluctuations. Therefore, if $\tau \gg \tau_c$ the intensity at time t and $t+\tau$will not be correlated. Thus, we can write

$$I(t) = \langle I\rangle + \Delta \mathrm{I}(t) \tag{2.7}$$

and

$$\langle I(t)\, I(t+\tau)\rangle = \langle (\langle I\rangle + \Delta \mathrm{I}(t))\,(\langle I\rangle + \Delta \mathrm{I}(t+\tau))\rangle$$

$$\langle I(t)\, I(t+\tau)\rangle = \langle I\rangle^2 + \langle I\rangle \langle \Delta \mathrm{I}(t)\rangle + \langle I\rangle \langle \Delta \mathrm{I}(t+\tau)\rangle + \langle \Delta \mathrm{I}(t)\, \Delta \mathrm{I}(t+\tau)\rangle$$

$$\langle I(t)\, I(t+\tau)\rangle = \langle I\rangle^2 \tag{2.8}$$

Therefore, second-order correlation function becomes

$$g^{(2)}(\tau \gg \tau_c) = \frac{\langle I(t)\, I(t+\tau)\rangle}{\langle I(t)\rangle^2} = \frac{\langle I(t)\rangle^2}{\langle I(t)\rangle^2} = 1 \tag{2.9}$$

If $\tau \ll \tau_c$ and $\tau = 0$, we can write

$$g^{(2)}(0) = \frac{\langle I(t)^2\rangle}{\langle I(t)\rangle^2} \tag{2.10}$$

It can be seen that for any reasonable time dependence of intensity, we can write

$$g^{(2)}(0) \geq 1 and g^{(2)}(O) \geq g^{(2)}(\tau)\,. \tag{2.11}$$

Let's consider we have a monochromatic light source, perfectly coherent, and intensity is time-independent. The second-order correlation function will be $g^{(2)}(\tau) = 1$ for all $\tau$ values.

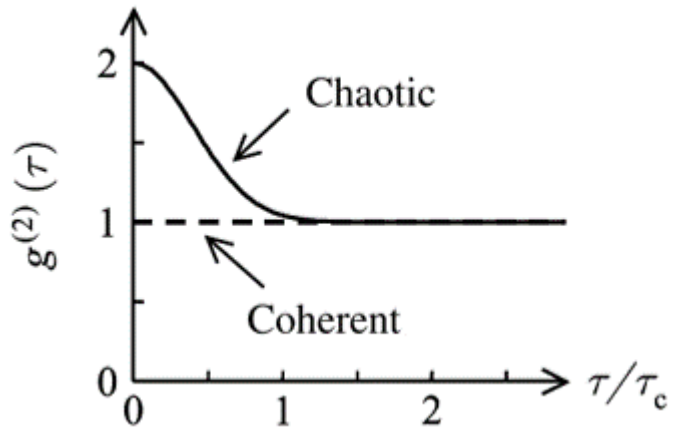


Figure 2.5: Second-order correlation function for a chaotic and coherent time [taken from Quantum Optics by Mark Fox]

If we have a light source that intensity values are time-dependent, we will have $g^{(2)}(0) > 1$. We can see that for any light source that intensity values are time-dependent we expect second-order correlation function values to decrease with $\tau$. On the other hand, if intensity values do not change in time we will have a constant value of second-order correlation function.[52]

The fluctuation in the intensity values and the photon correlations in coherent light was first studied by Hanbury Brown and Twiss in 1956,[69] later photon antibunching was observed by Kimble et al.[70] If we study Hanbury Brown and Twiss interferometer experiment with photons, we will see that equation 2.11 is not always the case. There is another light source that second-order correlation function smaller than one, ($g^{(2)}(0) < 1$) which indication of the quantum nature of the light.[52]

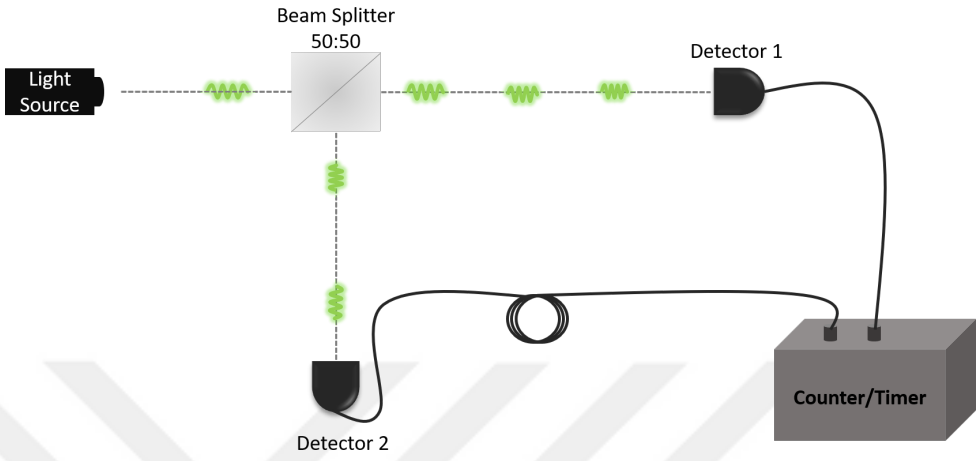


Figure 2.6: Experimental set-up of the Hanbury Brown - Twiss interferometer.

## 2.6 Hanbury Brown – Twiss Experiments with Photons

To understand the quantum nature of the light now we will study Hanbury Brown – Twiss (HBT) interferometer experiment. HBT interferometer construction can be seen in figure 2.6. There is a 50:50 beam splitter which is an optical instrument that either reflects or transmits the incoming photon. Thus, the incident light beam is equally distributed and sent to single-photon detectors. Detectors produce electrical pulses after interacting with the incident photons and are sent to the counter. There are two input ports connected to the detectors, the timer counts the number of pulses at each input while recording the time gap between each pulse coming from D1 and D2. In other words, the timer counts the coincident events. The experimental results give us information about the number of incidents at each time interval. Now, we can rewrite the definition of the second-order correlation function that is given in equation 2.6 as:

$$g^{(2)}(\tau) = \frac{\langle n_1(t)\, n_2(t+\tau)\rangle}{\langle n_1(t)\rangle \langle n_2(t+\tau)\rangle} \tag{2.12}$$

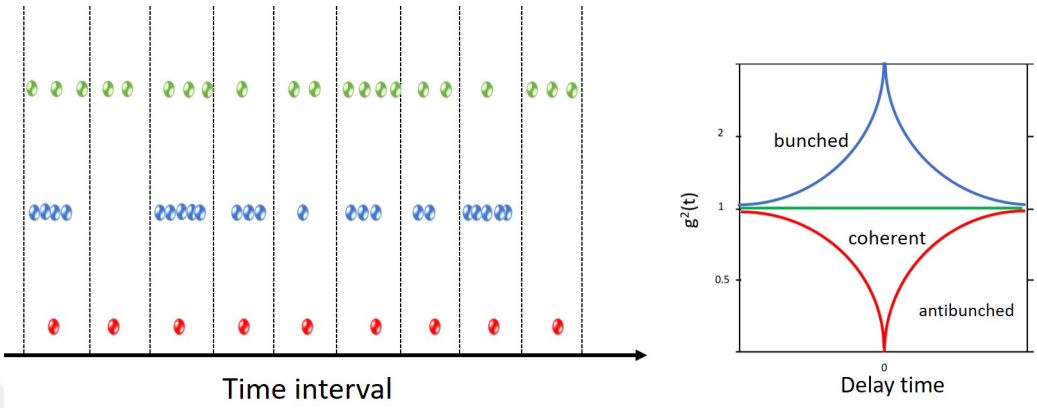


Figure 2.7: Schematic illustration of different results from the HBT experiment and second-order correlation functions.

where n (t) is the number of counts recorded on detectors at time t. This indicates that the second-order correlation function is determined via the probability of counting photons on detector 1 at t and detector 2 at time t + $\tau$ concurrently. Hanbury Brown – Twiss's experiment with photons can give us different results. Single-photon detectors D1 and D2 are connected to the timer via port 1 and port 2, respectively. Let's assume that the light beam consists of photons and the time interval between consecutive photons is long. Photons strike the beam splitter one by one. There is a 50 % chance that the photon will be reflected or transmitted, as a result, the photon either hit detector 1 or detector 2. If the photon hit detector 1, it will trigger port 1, and the timer records and the probability of obtaining a pulse from detector 2 will be zero. Therefore, there will be no coincident event that is recorded by the timer at $\tau = 0$. The next photon may hit detector 2 and trigger port 2 but we never expect to observe any event at $\tau = 0$. Therefore, we can say that we expect no event when $\tau = 0$, however, there might be coincident for larger $\tau$ values, which conflicts with the classical results that are given in equation 2.11. The results that we obtain from the HBT experiment with photons $g^2(0) = 0$ can only be explained by the quantum theory of light.

We can categorize the light depending on the second-order correlation function values:

- bunched light: $g^2(0) > 1$,
- coherent light: $g^2(0) = 1$,
- antibunched light: $g^2(0) < 1$.[71, 50]

Coherent light that corresponds to the Poissonian statistics is randomly distributed (time intervals between photons are not the same) and the second-order correlation function $g^2(0) = 1$ and for all $\tau$ values $g^2(\tau) = 1$. The bunched light distribution shows us that photons are clustered and there is a possibility of observing coincident events at $\tau = 0$. Thus, second-order correlation function is $g^2(0) > 1$. In antibunched light, photons are distributed regularly. The time interval between successive photons is equal and $g^2(0) < 1$. The light source emits one photon at a time which shows the quantum nature of the photons. Therefore, the materials that emit antibunched photons are defined as a single-photon sources.[52]

## 2.7 Single-Photon Emission

To test Bell's inequality theorem Clauser and Freedman performed experiment and for the first time entangled photons sources were discovered in 1972.[72] A few years later single-photon sources were demonstrated.[73] A photon source that shows non-classical behavior plays an essential role in quantum technologies 1, namely single-photon transistors[74], quantum key distribution [75], single-photon emitting diode [76], quantum internet [77], quantum coputing [78], and quantum sensing [79].

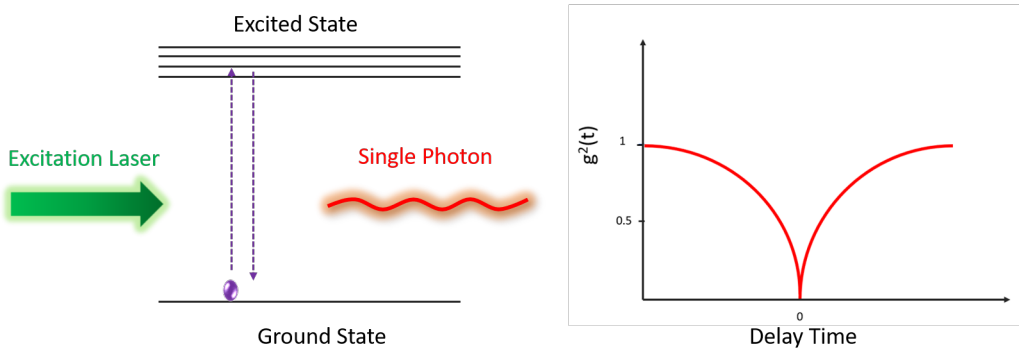


Figure 2.8: Schematic illustration of the single-photon emission and the second-order correlation function which indicates non-classical behavior.

Quantum technologies correspond to quantum physics and demand single-photon emitters to emit bright [80], inditinguishable [81], and pure [82] photons. Since the discovery of the single-photon various experiments have been performed and different materials and their photophysical properties have been studied as a single-photon source. There are several materials known as a single-photon source or in other words quantum emitters such as color centers in diamonds [83], quantum dots [84], single-walled carbon nanotubes [16], rare-earth doped crystals [85], and 2D layered van der Waals materials (transition metal dichalcogenides and hexagonal boron nitride) [86].

Single-photon can be created by spontaneous emission. As we can see in figure 2.8, a quantum system is excited with a laser and an electron jumped to upper state before returning to the ground state electron will state in the excited state which is called lifetime. When the electron returns to the ground state a photon is emitted. The emitted photon will be sent to the HBT set-up which will give us information about the second-order correlation function. If we observe a dip at zero, we can say that the emitted photon is non-classical light.[31]

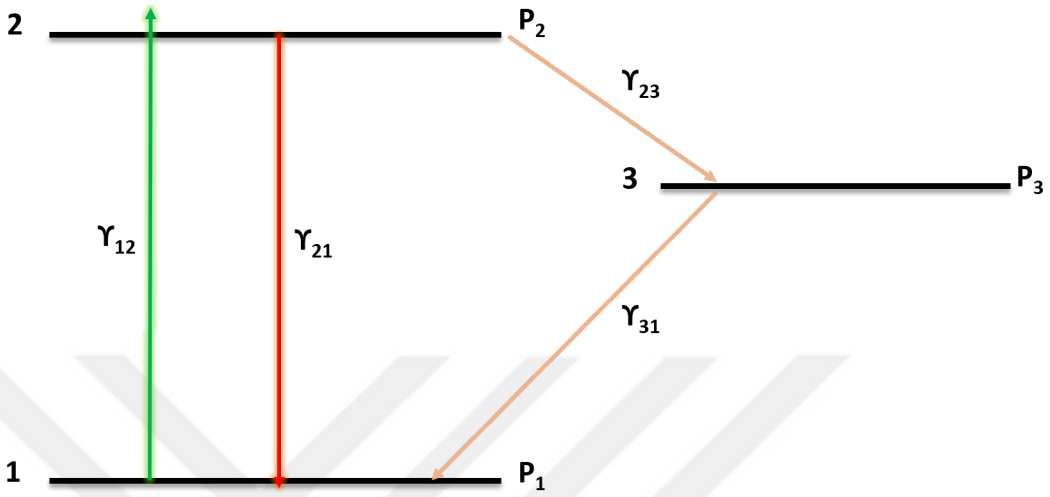


Figure 2.9: Schematic illustration of single-photon emission by the three-level system

### 2.7.1 Single photon emission by three-level systems

To study single photon emission from quantum emitters let's ignore the fast relaxation within the vibrational levels and simplify the Jablonski diagram. We get a three-level system, namely the singlet ground state, the singlet excited state, and the triplet state which are indicated by 1, 2, and 3 as can be seen in figure 2.9. The third level stands for triplet state or dark states. Excitation and relaxation processes emerge within these three levels. We can write a formula that shows the population change ($p_i$ , i = 1, 2, 3 ) for each level by using the excitation and relaxation rates.

$$\dot{p}_1 = -\gamma_{12} p_1 + (\gamma_r + \gamma_{nr})\, p_2 + \gamma_{31} p_3 \tag{2.13}$$

$$\dot{p}_2 = \gamma_{12} p_2 - (\gamma_r + \gamma_{nr} + \gamma_{23})\, p_2 \tag{2.14}$$

$$\dot{p}_3 = \gamma_{23} p_2 - \gamma_{31} p_3 \tag{2.15}$$

$$1 = p_1 + p_2 + p_3 \tag{2.16}$$

The last equation 2.16 guarantees and tells us that the emitter is in one of the three states at any time. The de-excitation rate has a radiative and non-radiative contribution.[87]

## 2.8 Single-photon emission in molecular perspective

In the molecule, there are possible transitions between rotational, vibrational, and electronic states. The rotational and vibrational states occur within electronic states. Typically, rotational transitions emerge in the microwave region, vibrational transitions emerge in the infrared region, and electronic transitions emerge in the visible or UV region. Therefore, the optical properties of the molecules can be split in three spectral regions:

- The far-infrared spectra: wavelength $\lambda > 100$ µm.
- The infrared spectra: wavelength $\lambda > 1 - 100$ µm.
- The visible and ultraviolet region: wavelength $\lambda < 1$ µm.

Figure 2.10 shows the molecular energy versus internuclear seperation (r). In a molecule there are electronic states, which optical transitions emerge. Within the electronic states, there are vibrational and rotational states. When an electron is excited and jumped to excited state and then return the ground state, raditaive an non-radiative transitions emerge.

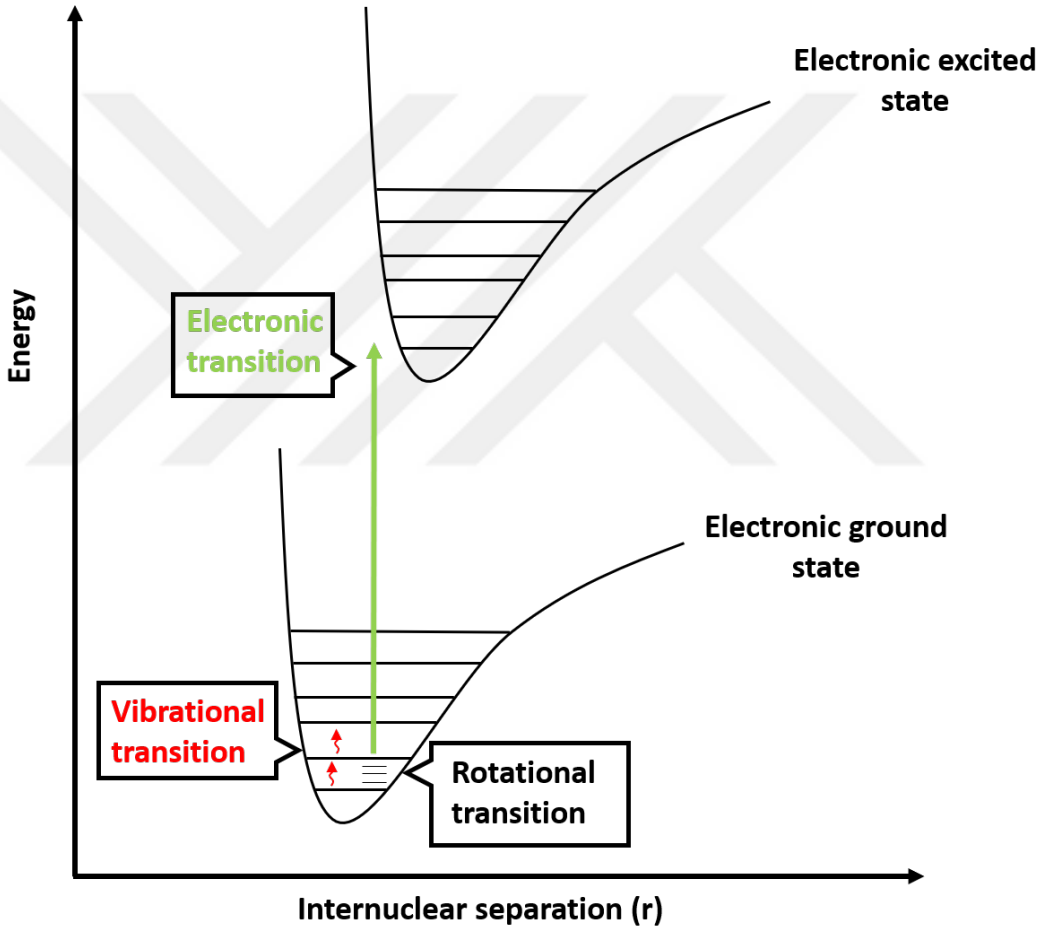


Figure 2.10: Demonstration of the molecular energy versus intergeneration curves and transitions. Green arrow indicates the electronic transitions. The red arrows show the vibrational transitions and black straight lines within the vibrational levels shows the rotational transitions

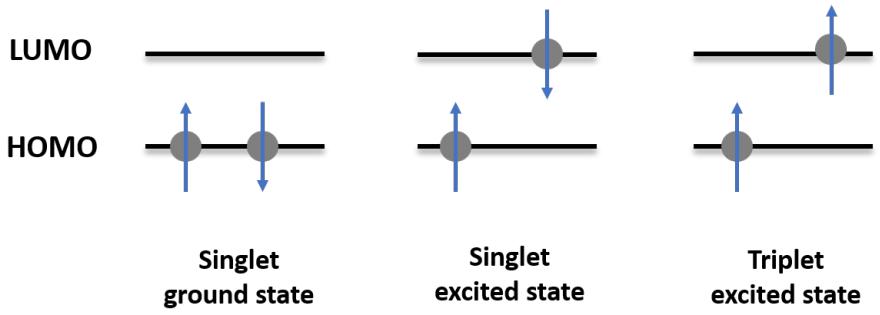


Figure 2.11: Illustration of the spin multiplicity

### 2.8.1 Electronic states and transitions

Arrangement of the molecular electronic states occurs the same way as the atoms. The electrons are located in the molecular orbitals. The highest occupied energy level is named HOMO which stands for highest occupied molecular orbital, state. The next energy level above the HOMO level is named LUMO which stands for the lowest unoccupied molecular orbital, * state. The lowest energy transition occurs from the $\pi$ state to the $\pi^*$ state which is labeled as $\pi \rightarrow \pi^*$.

Electrons are fermions and the spin value of an electron can be $\pm$ 1/2. When all the electrons are paired and the total spin value is equal to zero (S = 0) the state is called the singlet state, meanwhile, if there are unpaired electrons and the total spin value is equal to one (S = 1) the state is called the triplet state. In the case of the triplet state, there will be degenerate energy levels. this spin multiplicity is very important. When the singlet state passed to the triplet state or vice versa nonradiatively, this process is called intersystem crossing (ISC). This process involves spin-orbit coupling and allows us to study spin electronics properties.[88, 89]

### 2.8.2 Vibronic transitions

When an electronic transition emerges in the molecule, there is likely a vibrational transition as well. We can see the vibrational-electronic transitions in figure 2.12. It is assumed that ground and excited states are singlets, thus electric-dipole transitions are allowed. In the figure the process tagged 1 is absorption and 3 is emission, electronic transitions occur between the ground state and excited state. Processes numbers 2 and 4 are vibrational transitions (non-radiative relaxation). When the atoms in the molecule vibrate they produce thermal energy and the quantization of thermal energy is called a phonon. The angular frequency of the vibrational oscillation is given by $\Omega$ and the vibrational energy is given via $(n + 1/2)\ \hbar\ \Omega$ formula, n quantization numbers of vibrational energy (n = 0,1,2,...). Therefore, the total energy of the molecule in the ground state is given by:

$$E_g = E_1 + \left(n_1 + \frac{1}{2}\right)\hbar\Omega_1 \tag{2.17}$$

The total energy of the molecule in the excited is given by:

$$E_e = E_2 + \left(n_2 + \frac{1}{2}\right)\hbar\Omega_2 \tag{2.18}$$

The optical transition occurs when an electron jumps from a ground state to an excited state by absorbing a photon. The absorption process is shown in figure 2.12 and indicated with 1. We accept that molecule is in the lowest vibrational energy level before the absorption emerges.

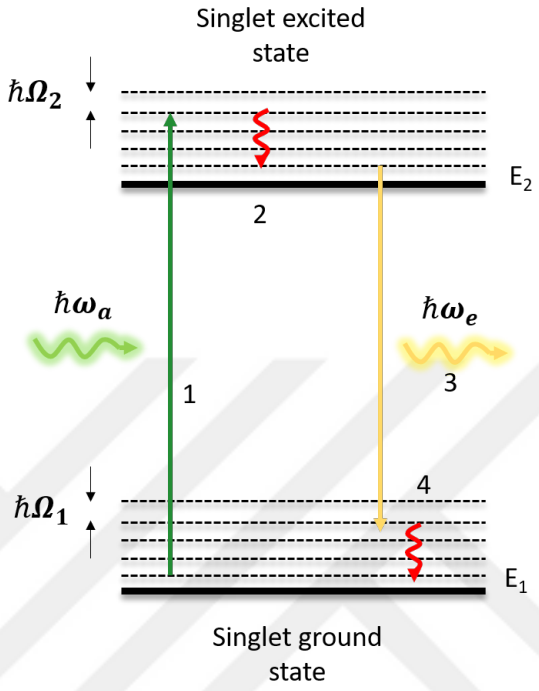


Figure 2.12: Schematic illustration of the vibrational-electronic transitions in a molecule.Processes 1 and 3 are respectively absorption and emission and 2 and 4 are non-radiative relaxations.

The energy of the absorbed photon can be written as:

$$\hbar\omega_a = \left(E_2 + \left(n_2 + \frac{1}{2}\right)\hbar\Omega_2\right) - \left(E_1 + \frac{\hbar\Omega_1}{2}\right)$$

$$\hbar\omega_a = \hbar\omega_0 + n_2\hbar\Omega_2 \tag{2.19}$$

where $\omega_a$ is the angular frequency of the absorbed photon and

$$\hbar\omega_0 = E_2 - E_1 + \frac{1}{2}\hbar\left(\Omega_2 - \Omega_1\right) \tag{2.20}$$

When a photon is absorbed by a molecule, a vibrational-electronic transition occurs and the electron jumps to an excited electronic state, and meanwhile, excess vibrational energy will be produced. As we can see in figure 4.9 process tagged 2 non-radiative relaxation emerges in the excited electronic state and extra energy will be given to the system as heat. After the extra energy is given to the system, the molecule will be relaxed to the bottom of the excited state. Then the electron will return to the ground electronic state by emitting a photon which is shown in the process 3. The energy of the emitted photon can be written as:

$$\hbar\omega_e = \left(E_2 + \frac{\hbar\Omega_2}{2}\right) - \left(E_1 + \left(n_1 + \frac{1}{2}\right)\hbar\Omega_1\right)$$

$$\hbar\omega_e = \hbar\omega_0 - n_1\hbar\Omega_1 \tag{2.21}$$

Finally, the molecule will be returned to the ground state giving the extra vibrational energy to the system via non-radiative relaxation in process 4. When we look at equations 2.19 and 2.21 we can see that absorption photon energy is higher than the emitted photon energy due to the energy loss via non-radiative relaxations. The energy difference between absorbed and emitted light is called Stokes shifts. To understand vibrational-electronic spectra of molecules we will think of a simple diatomic molecule, the Born-Oppenheimer approximation says that electronic and nuclear motions are dependent. This means that we can draw the electronic energy states as a function of internuclear separation as we can see in figure 2.10. this approximation is reasonable because nuclei are much heavier than electrons, hence they move much slower time scale. Due to the Coulomb interaction and Pauli exclusion principle there are intermolecular forces, namely attractive and repulsive forces. Thus, there is a certain distance that two nuclei of a molecule can get close which is indicated by r. When the distance is large enough between the atoms, because of attractive forces atoms will get close to each other. However, if they get too close then due to the electron-electron and proton-proton repulsion, atoms will move apart from each other again. The separation of the two nuclei for the ground state is labeled as r1 which corresponds to the equilibrium separation for the unexcited molecule.

When the molecule is excited the mean separation of the nuclei is labeled as $r_2$. Generally, $r_1$ and $r_2$ are not the same because the radius of one of the atoms increases in the excited state.

### 2.8.3 The Frank-Condon principle

To understand the optical transition between the coupled vibrational-electronic level of a molecule now we will look at the Frank-Condon principle. The Frank-Condon principle agrees with the Born-Oppenheimer approximation and says that electrons move faster than nuclei because they are lighter. In addition to electronic transitions, molecular spectra also illustrate the vibrational degree of freedom.

According to the Franck-Condon principle, optical transitions in the molecule are shown with vertical arrows, the green arrow represents the absorption and the red arrow represents the emission, and the non-radiative relaxations are shown with a black dashed line in figure 2.13. The Franck-Condon principle defines the intramolecular vibrations and the coupling of the lattice modes (phonons) to electronic transitions. The vibrational motions are defined by normal lattice modes (Q). We can produce and draw electronic energy as a function of Q. As is shown in figure 2.13, when an electron is excited and jumped from the ground state to the excited state ($E_0 \rightarrow E_1$), the equilibrium distance will be changed from $Q_0$ to $Q_0$'. We can calculate the probability of transition from the ground state to the excited state by using the Frank-Condon principle.

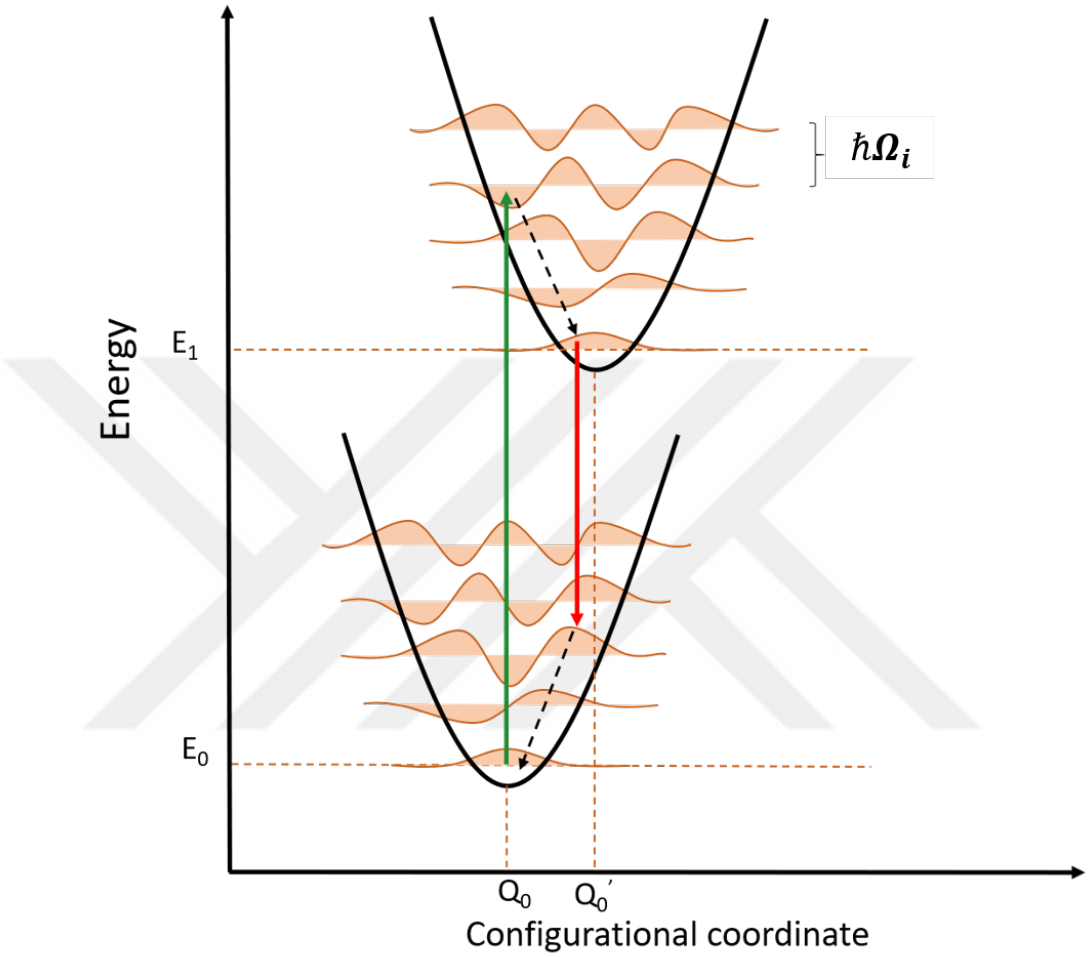


Figure 2.13: Frank-Condon configuration diagram for vibrational-electronic levels in a molecule. Vertical arrows indicate the photon absorption and emission.

The Franck-Condon principle states that electronic transitions do not change the atomic configuration because electronic transitions happen so fast that lattice coordinates cannot follow. The probability of optical transition in electronic states can be calculated via Fermi's golden rule:

$$P = \frac{2\pi}{\hbar} \left|\langle \Psi_1 \left| H_{rad} \right| \Psi_0 \rangle\right|^2 g\left(E - E_1\right) \tag{2.22}$$

The Franck-Condon principle and coupling of the lattice mode to electronic states, the transition probability from the lowest vibrational state to the vth level of the lattice mode $Q_0'$ in the excited state can be calculated as:

$$P(v) = \frac{2\pi}{\hbar} \left|\langle \Psi_1 \phi_1(v) \left| H_{rad} \right| \Psi_o \phi_0(v) \rangle\right|^2 g(E - E_1 - v\hbar\Omega_i) \tag{2.23}$$

$\Psi_0$ and $\Psi_1$ are the wave functions of electronic ground state and the electronic first excited state, respectively. $\phi_0$ and $\phi_1$ are the vibrational levels and g is the normalized line shape function.[88, 90]

## 2.9 Zero-phonon lines and phonon sidebands

Now let's think of a vibronic transition where vibrational quantum numbers are v1 and v2 for initial and final states. The intensity of the vibronic transition can be calculates by:

$$I \propto \left|\langle v_2, Q_0' | v_1, Q_0 \rangle\right|^2 \tag{2.24}$$

The square of the vibrational overlap is called the Frank-Condon factor. Only several vibrational modes are strongly coupled to the optical transition with the largest Frank-Condon factor. The line shape function, g in equation 2.23 causes the narrow peaks, and the space between them are determined by $\hbar\Omega_i$ The overlap of the harmonic oscillator wave functions determines the intensity of those narrow peaks. Figure 2.14 a) and b) demonstrate the transition probabilities for two different modes, i and j. In figure c) we see the emission and absorption spectrum obtained from the superposition of mode I and mode j. Even though the intensity mode i and j assemble at the zero-phonon line frequency, they do not assemble in the multi-photon transitions.

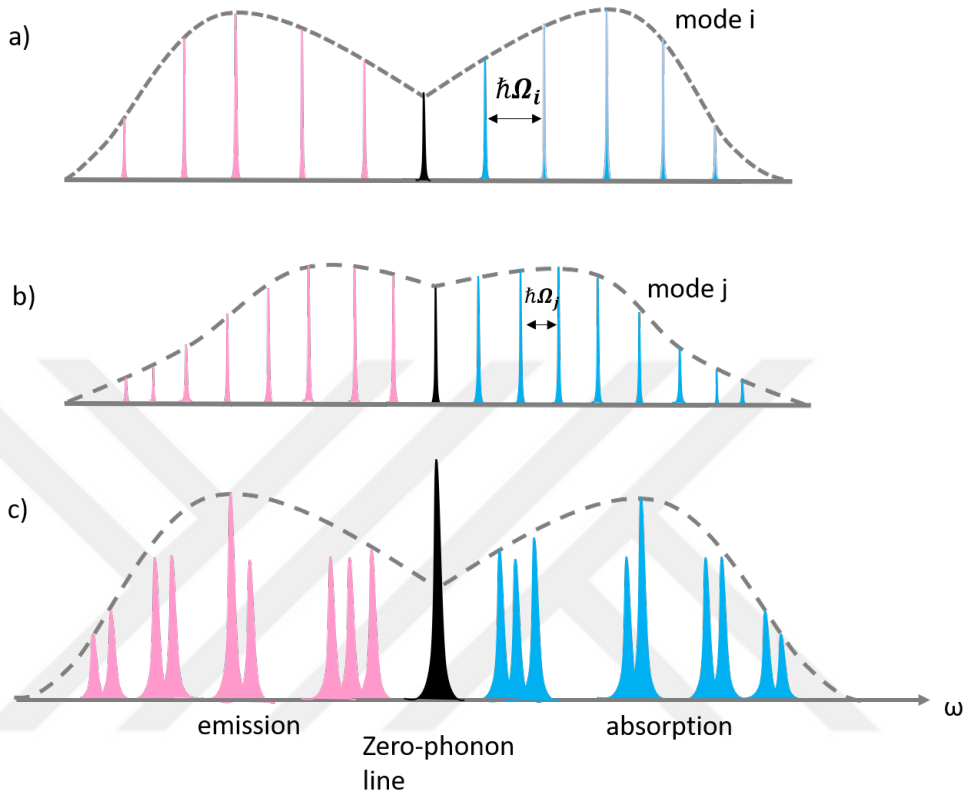


Figure 2.14: Demonstration of the transition probabilities for modes i and j in (a,b). c) Superposition of mode i and mode j.

The whole spectrum is predominated via the zero-phonon line. There are two reasons for that. At first, the linewidth of the zero-phonon line is narrower because its relaxations are forbidden to a degree. Secondly, the zero-phonon lines of all the lattice modes assemble at the electronic origin. The envelope of all phonon excitations determines the phonon sideband. [88, 90]

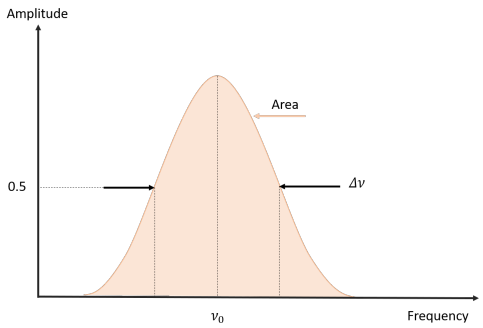


Figure 2.15: Simple illustration of a lineshape as a function of frequency.

## 2.10 Lineshape of optical spectra

The radiation in optical transitions is not monochromatic. The lineshape of emission spectra is determined via normalized lineshape function g(). The peaks at the line center is determined by

$$\hbar\omega_0 = E_2 - E_1 \tag{2.25}$$

and normalized lineshape function is

$$\int_0^\infty g(\omega)\, d\omega = 1. \tag{2.26}$$

The maximum value of a lineshape is located at the center frequency ($\nu_0$). The width of the lineshape is quantified via full width at half maximum (FWHM) $\Delta\nu = \Delta\omega/2\pi$. The line broadening emerges as a result of physical processes that happen during the optical transitions. Individual atoms or molecules interact with light. If this interaction affects all atoms in the medium, in the same way, the line broadening is defined as homogenous. On the other hand, if various interactions occur, this is defined as inhomogeneous broadening. There are different broadening mechanics, namely natural (lifetime) broadening, pressure broadening, and Doppler broadening. Natural and pressure broadening mechanisms are homogenous broadening, while doppler broadening is inhomogeneous[52].

### 2.10.1 Spectral diffusion

Charge fluctuation in the vicinity of the emitter causes the Stark effect, thus sudden jumps occur in the emission energy over time. In the range of nanoseconds to milliseconds, energy shifts appear. Most of the solid-state single-photon emitters suffer from spectral diffusion including, quantum dots, color centers in diamond, and two-dimensional materials. Spectral diffusion also leads to inhomogeneous broadening. Obtaining stable emission is very important for both optoelectronic and quantum photonic technologies. Therefore, we investigated the photostability of the quantum emitters, and we will mention it in the experimental part.[91, 92]

## 2.11 Quantum emitters in hexagonal boron nitride

The study of atomically layered material has grown rapidly, since the discovery of graphene. The impact of the change from 3D to 2D confinement on the optical, electrical and mechanical characteristics of 2D materials has been recently investigated. Researchers have been drawn to hexagonal boron nitride (h-BN) because of its distinctive properties. Even when formed into a monolayer, bulk hBN crystals demonstrate exceptional chemical stability and can be exfoliated down to a single atomic layer. Its new material features allow for a variety of optical, electro-optical, and quantum photonics capabilities.[35]

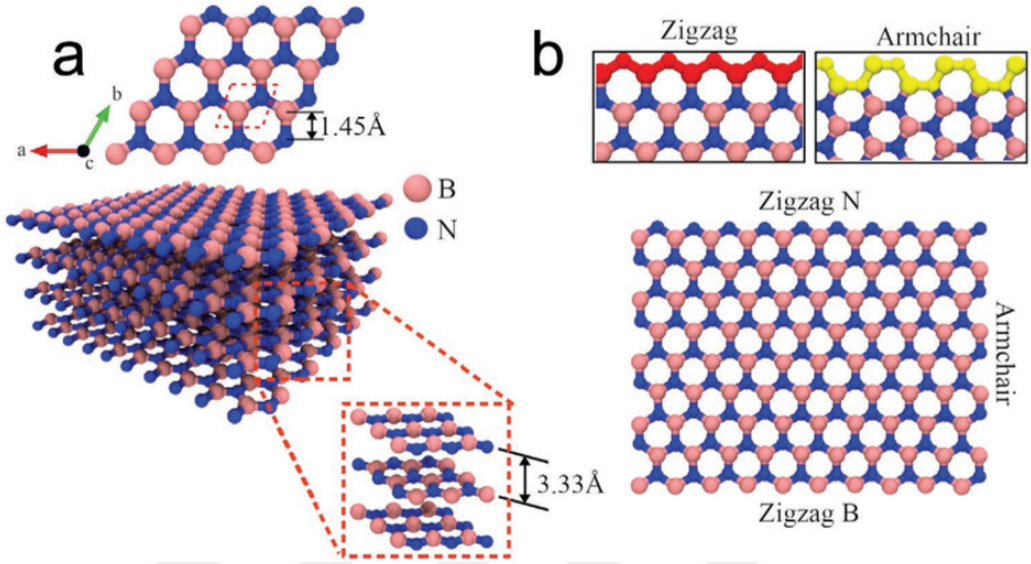


Figure 2.16: a) The schematic illustration of the h-BN crystal structure. b) Demonstration of atomic distribution. [S.Roy et al. Adv.Matter 2021,33,2101589]

### 2.11.1 Structure and Properties of Hexagonal Boron Nitride

Hexagonal boron nitride (h-BN) is a chemical composition with equal number of boron and nitrogen atoms arranged honey-comb structure similar to the graphene. h-BN consists of highly polarized and strong covalent B-N bonds and van der Waals interactions (vdW) between atomic layers[93, 94]. It has a flat surface, hence almost free of dangling bonds and surface charge traps [95, 96]. Figure 4.13 shows the schematic structure of the h-BN crystal lattice. The distance between layers is 3.3 Å and the bond length is 1.45 Å. Depending on the arrangements, atoms are allocated in a zigzag and armchair configuration [97]. In the form of mono and a few layers, h-BN shows stability, and due to the crystalline configuration different unique properties emerge, thus attractive to researchers. h-BN has high thermal conductivity and mechanical strengt [98].

Due to its crystalline structure h-BN shows anisotropic, excellent mechanical strength, and high chemical stability. Those extraordinary properties make h-BN an ideal candidate for nano-device applications [99, 100, 101]

### 2.11.2 Electronic and Optical Properties

Hexagonal boron nitride has a wide bandgap. To understand its band structure both experimental and theoretical studies have been performed. Studies indicate both direct and indirect bandgap varies from 3.6 to 7.1 eV [102]. The bandgap of h-BN can change depending on the dimension, size, purity, etc [103, 104]. Theoretical work has been done to see the relation between bandgap and thickness of the h-BN crystal. Wickramaratne et al. studied how bandgap changes depending on the number of layers by using first-principle calculations. When the number of h-BN layers increases the bandgap structure changes from direct to indirect [105]. This theoretical work is also in agreement with experimental results [93, 106].

The electronegativity of N atoms is higher than B atoms, the electrons in $sp^2$ hybridized B-N bonds cannot be allocated, and thus highly polarized b-N bonds emerge. As a result of this, h-BN acts as an insulator [107]. Due to the large bandgap h-BN can be used as a dielectric in heterostructure electronic device [108].

Even though, its wide bandgap, h-BN gives emissions at a deep-ultraviolet range due to the strong electron-phonon interaction, hence a potential candidate for optoelectronic technologies [109, 110]. h-BN also hosts quantum emitters that can be used in quantum technologies [111].

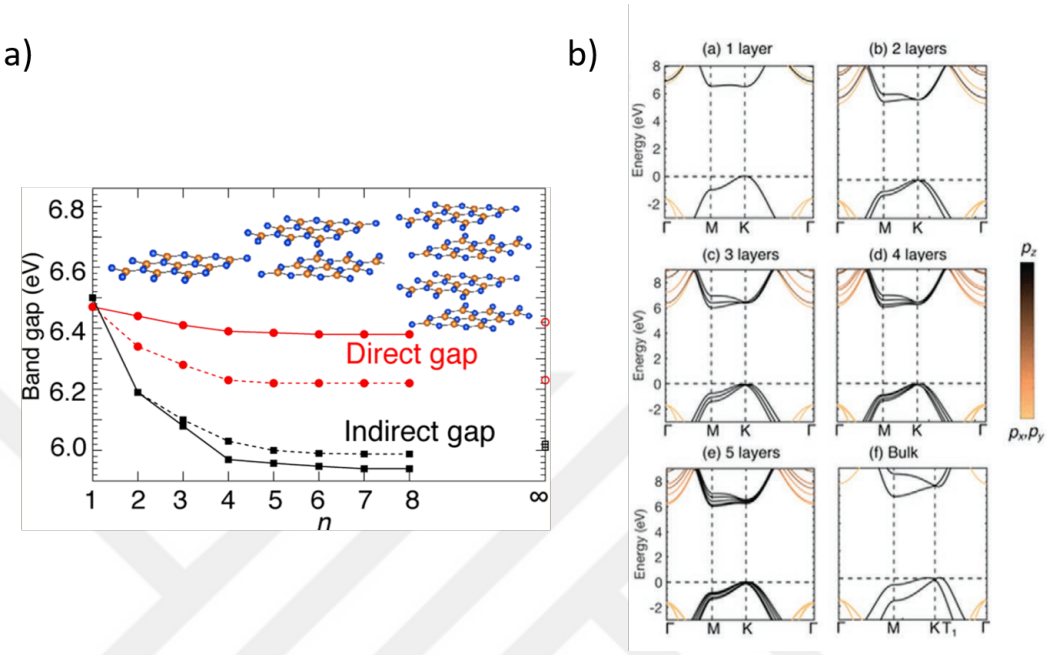


Figure 2.17: a) The bandgap relation with the thickness of h-BN layers. b) The band structure in AA' stacking configuration from monolayer to bulk.[Wickramaratne et al. Phys.Chem.C 2018]

### 2.11.3 Single Photon Emission from Hexagonal Boron Nitride

Although h-BN has a wide bandgap, studies show that single-photon emission emerges from h-BN in both UV and visible ranges. The origin of single-photon emission is still under debate; however, it is attributed to the presence of various defect centers in h-BN. The bandgap and structure vary depending on the dimension, and size and can be tuned via different defect centers such as vacancy defect (VB, VN), impurity (CB, ON), antisite defect (NB), substitutional antisite defect (VNCB), etc. [112, 113, 114, 115] Single-photon generation can be achieved from those optically active defect centers.

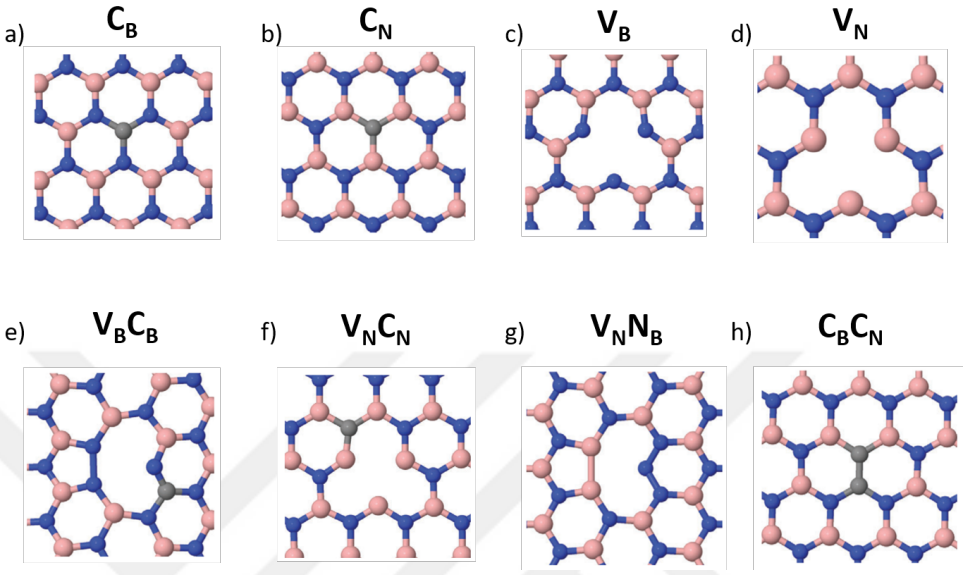


Figure 2.18: Schematic illustration of various possible example defects in h-BN. [Korona et. al. Int J Quantum Chem. 2019;119:e25925]

Therefore, h-BN is one of the promising solid-state single-photon emitters that can be used for quantum photonic device applications. Photoluminescence (PL) studies illustrate that h-BN gives various PL emissions, and this strongly suggests that occurrence of different defect centers. We can see schematic diagrams of some of the possible defect centers in h-BN. Figure 2.18 illustrates the schematic diagram of different possible defects centers. The first type is called substitutional defect which can be formed when one carbon atom is replaced by one boron (CB) or one nitrogen (CN). The second type of defect is vacancy defect which can be produced by removing one nitrogen (VN) or boron (VB) atom. Other types of defects can be formed by the combination of defects. For example, when one nitrogen atom is removed and the boron atom is displaced by one nitrogen atom (VNNB), or one nitrogen atom is removed and another nitrogen atom is displaced with carbon (VNCN). All these defect centers create deep-defect levels between the valance band and conduction band, hence sing-photon emission emerges from that deep-defect levels [116, 117, 118].

Single-photon emission in h-BN is attributed to those deep-defect levels between valance and conduction band. However, the origin of quantum emitters in h-BN is still under debate. A variety of h-BN materials hosts quantum emitters, including mechanically exfoliated flakes, commercially available flakes, and growth flakes. different experimental methods have been used to create optically active defect centers, including thermal annealing, electron irradiation, ion irradiation, and chemical etching. In this thesis work, we used commercially available solution-based h-BN flakes.[119, 38, 120]

# Chapter 3

# Experimental Measurement Systems

In this work, we used commercially available (purchased from 2D Semiconductors) solution-based h-BN flakes. The flakes' thickness varies from 1 to 10 atomic layers, and 10 nm to 10 mm in lateral size. We used acetone, isopropanol, and distilled water to clean the substrate before drop-casting h-BN solution onto a SiO2/Si substrate. After the substrate has been cleaned, we drop-cast h-BN solution onto it and allow it dry for the night in atmospheric conditions. Figure 5.1 illustrates the sample preparation and the annealing process. To create optically active defect centers, the samples were then annealed for 30 minutes at 850 °C and 1 Torr argon pressure (Protherm Furnace PC 442). First, we started with optical characterization at room temperature to check whether we created optically active defect centers or not for that we used Raman Confocal Microscope (WITec). After its initial optical characterization at room temperature, we further investigated the photophysics of those emitters at low temperature by using the home-built low-temperature micro-PL setup.

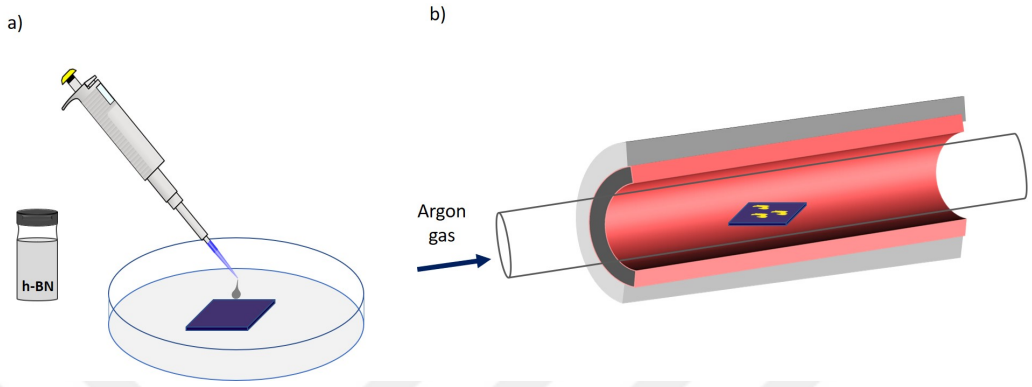


Figure 3.1: Schematic illustration of the sample preparation process. a) Shows that we drop-casting h-BN flakes in ethanol onto SiO2/Si substrate. After drop-casting the solution, we let the samples dry over a night under atmospheric conditions. b) We annealed the samples for 30 minutes at 850 °C, under 1 Torr argon pressure.

## 3.1 Optical characterizations at room temperature

As we discussed earlier, the origin of quantum emitters in hBN is under debate. However, it is considered that single-photon emission occurs due to the presence of deep-defect levels between valance and conduction band. There are various defect engineering methods and, in this work, we used the thermal annealing process to create optically active defect centers. Before we conduct low-temperature measurements with our home-built micro-PL setup, we used Raman Confocal Microscope (WITec) to perform room temperature optical characterizations (Raman spectroscopy, Photoluminescence spectroscopy). One of the main purposes is to see if there are enough defect centers to study and conduct further experiments.

### 3.1.1 Photoluminescence spectroscopy

The general principle the photoluminescence (PL) is we excite the sample using a probing light source. When we excite the sample, electrons jump from the ground state to excite state, and remain there for a while (lifetime of the excited state),

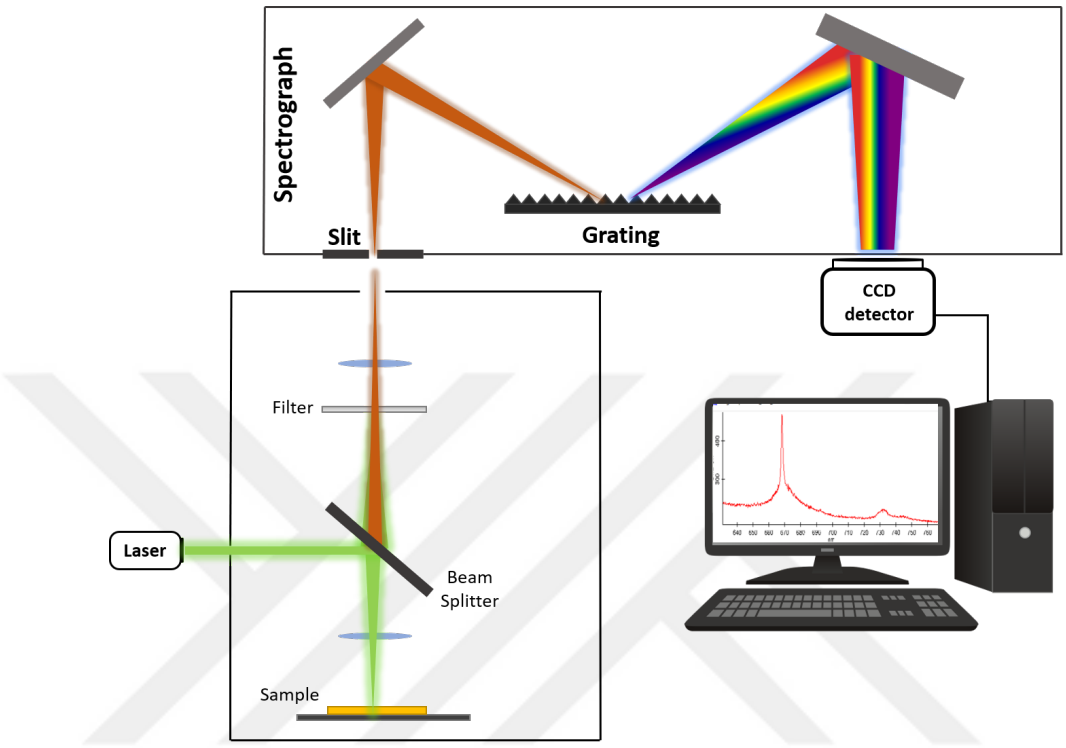


Figure 3.2: Schematic illustration of the Raman Confocal Microscopy. We used CW (532 nm) laser light for excitation. After the sample is excited, the emitted light is collected and sent to the spectrograph. There is a CCD camera attached to the spectrograph which is used to analyze the PL signals.

then return to the ground state by emitting photons. After that emitted light is collected to study.

The photoluminescence spectrum tells us about the energy difference between the valance band and conduction band, we can also learn the excitation, the radiative and non-radiative transitions, the lifetime of the PL signal, and we can study the quantum nature of the emitted light. Photoluminescence spectroscopy is a crucial instrument to characterize the electronic states and transition rates to specify the capability of quantum emitters for their usage in quantum photonics technologies. [121, 122]

After the sample preparation process is done, we conducted PL measurements at room temperature to search optically active centers in h-BN flakes. In figure 5.3 we see the diagram of the Raman Confocal Microscope and PL measurement. During the PL measurements, we used a continuous wave (CW) green laser (532 nm). We put our sample under the objective lens and excite the h-BN flakes with laser light. Then emitted light is collected and sent to the spectrograph via fiber. To blockade the laser light filter is used in the microscope setup. There is a grating in the spectrograph that is used to disperse collected light. There is a CCD camera attached to the spectrograph. The dispersed light is sent to the CCD camera to analyze the individual PL signals. When we hit the laser light onto an optically active defect center we see PL signals on the screen. h-BN has a wide bandgap and single-photon emission occurs in deep defect levels within the bandgap due to the presence of defect centers. Those defect centers are on the order of atomic scale and it is not possible to see under an optic microscope.

To be able to find those defect centers, first, we look at the sample and find the h-BN flakes. After that, we choose a starting point on one of the h-BN flakes and then start searching the defect centers as we excite the flakes. We do not see any PL signals unless we hit the defect centers. After searching h-BN flakes, we locate the positions of optically active defect centers and conduct the PL measurements.

## 3.2 PL and spectral diffusion measurements at low temperature

We performed various characterization techniques at low temperature by utilizing a home-built micro-PL setup, including photoluminescence spectrum, spectral diffusion, lifetime, and antibunching measurements. The h-BN sample we put within a closed-cycle cryostat (attoDRY 1000) with a based temperature of 3.5 K. As an excitation source, a picosecond pulsed laser diode at 532 nm was used in both the continuous wave (CW) and pulsed modes. After the excitation, the emitted light was collected by the microscope objective (0.82 NA) and

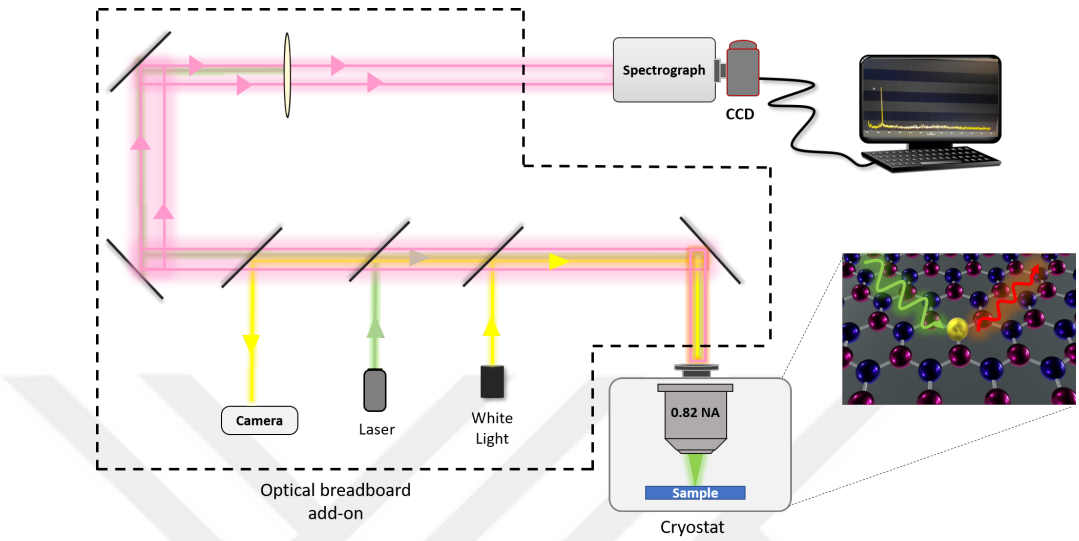


Figure 3.3: Schematic diagram of the home-built micro-PL setup. Under the microscope's objective, the sample is mounted on the nano-positioners in the cryostat. White light is used to find the sample surface and see the h-BN flakes. Mirrors are indicated with black solid lines. We blockade the collected PL signals by using the 550 nm long-pass filter coupled to a single-mode fiber. Then collected light was sent to the spectrograph and recorded PL signal.

coupled to a single-mode fiber after being filtered by a 550 nm long-pass filter. The PL spectra were recorded using a 750 nm focal length spectrograph (Princeton Instrument SpectraPro HRS-750) to which a liquid nitrogen-cooled silicon charged-coupled device (CCD) camera (PyLoN).

We found the sample's surface after mounting it on the nano-positioner controlled stage in the cryostat. Afterward, as we performed optical characterizations at room temperature, we first began searching the optically active defect centers in h-BN flakes. Optically active defect centers were activated during the thermal annealing process, however, because they are point defects, they can not be seen under an optical microscope. As a result, as we excite the h-BN flakes, we simultaneously look at the real-time spectrum on the screen and search for defects by using the X, and Y nano-positioners. If there are any defects, the PL signals appear on the screen as shown in figure 3.3. With this experimental setup, we measured spectral diffusion and recorded PL signals of defects centers. To conduct additional characterizations, we recorded the coordination of the defect

centers. The base temperature was set to 3.5 K. during the low-temperature characterizations we did not change the temperature.

The photos of the equipment that we used during PL and spectral measurements were taken and shown in figure 5.6 Optical breadboard mounted on a slider and located on the cryostat, thus when we want to put or take out a sample, we slide it over. To perform low-temperature measurements, first, we start putting a sample in the cryostat, as shown in figure 4.3.2 (c). To do that we remove the vacuum tube (d) from the cryostat. Before we do anything, we wait for the base temperature to reach room temperature, which approximately takes two hours. After that, there is a microscope stick inside the vacuum tube (f), we remove the stick from the vacuum tube and put on the holder, and fix it. At the bottom of the microscope stick, there is a microscope housing. Microscope housing hosts the necessary elements, objective lens (0.82 NA), positioners, and electrical connections to the microscope stick cable (g). We put our sample on the sample holder and locate it under the objective lens. Then we put the microscope stick back in the vacuum tube. Before we put the vacuum tube inside the cryostat we adjust the pressure of the tube. Then we put the vacuum tube inside the cryostat. Before starting any measurements, we wait for the base temperature to cool down to 3.5 K. The whole process of putting the sample inside the cryostat approximately takes 4 to 5 hours.

We put our sample on the sample holder and locate it under the objective lens. Then we put the microscope stick back in the vacuum tube. Before we put the vacuum tube inside the cryostat we adjust the pressure of the tube. Then we put the vacuum tube inside the cryostat. Before starting any measurements, we wait for the base temperature to cool down to 3.5 K. The whole process of putting the sample inside the cryostat approximately takes 4 to 5 hours. After placing the sample inside the cryostat and waiting for the temperature to cool down, we reach the surface of the sample, find the h-BN flakes, and focused the laser. During the defect searching, we used the nano-positioner.

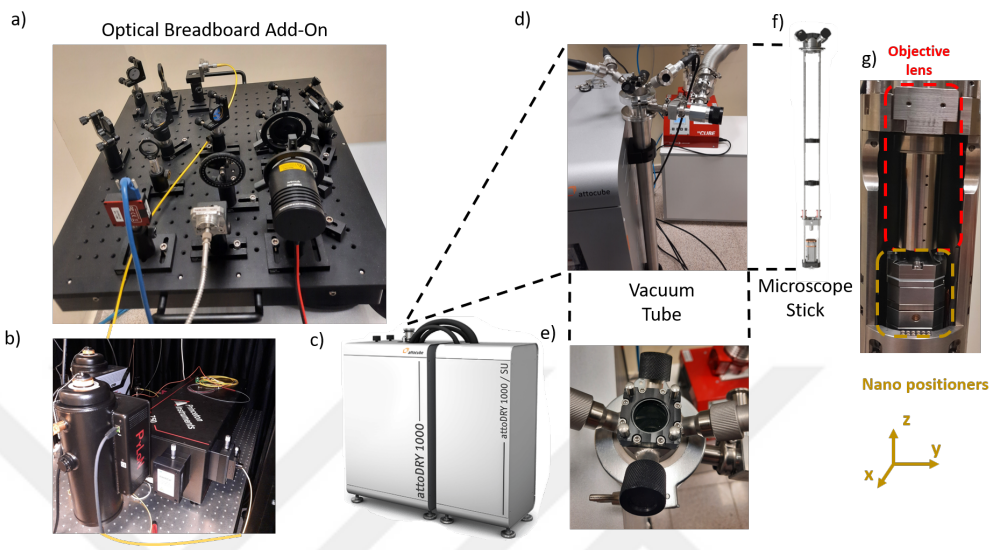


Figure 3.4: Real photos of the equipment that we used in our laboratory for PL and spectral diffusion measurements. a) Optical breadboard which was added to the cryostat. On the optical breadboard, starting from the lower right corner, we see the white light source, laser source, and camera, respectively. On the upper left corner, there is a mirror and right next to the mirror we see the 550 nm long-pass filter, after the filter emitted light is coupled to the single-mode fiber and sent to the (b) spectrograph. g) Shows the objective lens and under the objective lens, there is a sample holder which is controlled by the nano-positioner. f) Shows the microscope stick, at the top we see the microscope head which contains all the electrical connectors, and (e) the window that lets the light through, upper and lowers cage plates, and microscope holder, respectively. d) Shows the vacuum tube that we used to insert the microscope stick. c) Shows the cryostat that the vacuum tube is inserted.

## 3.3 Lifetime measurements at low temperature

Time correlated single-photon counting (TCSPC) is an incredibly capable and adaptable optical characterization technique. TCSPC utilizes the single quanta of light and gives information about the light's temporal structure. The idea of the TCSPC is to measure the time interval between the associated excitation light pulse and emission photon as measured by a single photon avalanche diode. The timer is started when the laser pulse strikes the sample, and when emitted photon is detected, the timer is stopped. This cycle is repeated over and over again. it is shown in figure 3.5 (a), sometimes no photon will be observed. The

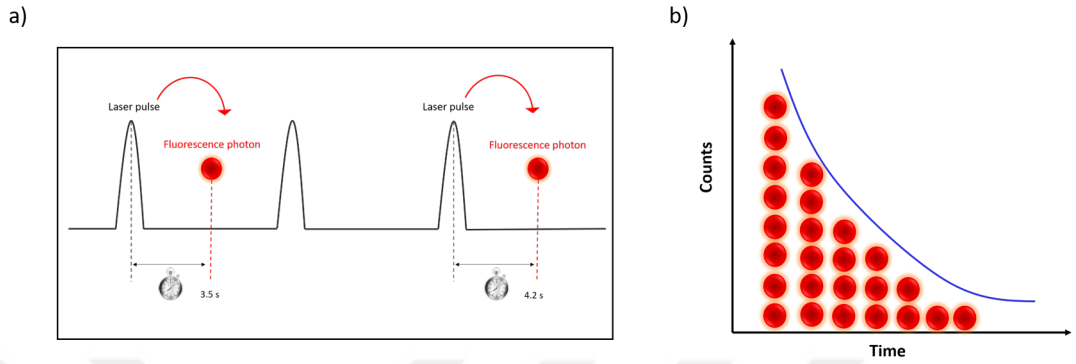


Figure 3.5: a) Schematic illustration of the measurement of start-stop time. b) Histogram plot of the start-stop times.

counts of the emission being observed are on the y-axis and all possible times on the x-axis.

Overall the cycles we get the histogram. The time that laser pulse is sent to excite the sample is recorded, then the time that emitted photon is observed recorded and this process is recorded. This cycle is repeated many times and the time differences that is collected from each cycle provides statistical data for the histogram plot shown in (b).

Figure 3.5 demonstrates the formation of the histogram plot. The time interval between the excitation laser pulse and the emitted photon is measured by timing electronics connected to a computer. Naturally, it takes a significant number of repetitions to fill the histogram to the point where the error resulting from counting statistics is minimal. The bottom end may be constrained by noise (stray light, detector dark counts), but TCSPC can still produce a dynamic range up to 106. Each data point corresponds to a histogram bin and we are counting photons and putting them in bins.As it is shown in figure 3.6, we have a laser diode driver that sends a signal to the laser head and the timing electronics. When the signal goes to the laser head, it will be triggered and sends a light pulse to the sample. Light pulse first goes through the neutral density (ND) filter which is used to attenuate the laser power, then hit the sample and excites.

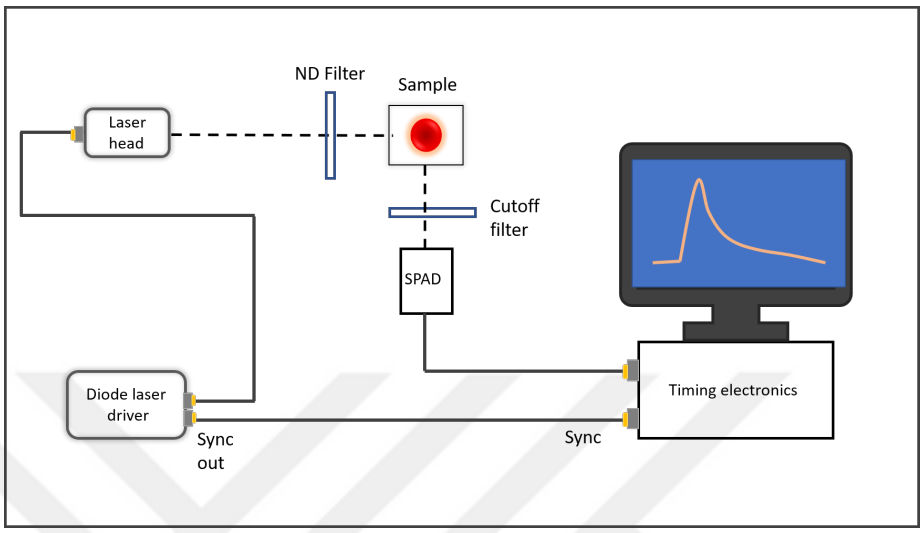


Figure 3.6: Diagram shows the time-correlated single photon counting.

As a result of excitation, photons are emitted. Then emitted light is collected and sent through the cut-off filter to prevent scattered light toward the detector. after the cut-off filter, it goes to the single-photon avalanche diode detector with a photon timing resolution of 50 picoseconds and then timing electronics (HydraHarp 400 multichannel picosecond even time). The time is recorded as a start timing when the diode laser driver sent a signal to the timing electronics, and the time is recorded as a stop timing when an emitted photon is observed. The cycle is repeated over and over, as a result, the histogram plot is formed as shown on the computer screen. Histogram data is used to calculate the lifetime of the excited state.[123, 124]

## 3.4 Antibunching measurements at low temperature

Antibunching measurement is a method that is used to determine the quantum nature of light. Consequently, it is employed to investigate the performance of solid-state single-photon emitters. The form of quantum light, known as antibunching, is one in which photons are separated from one another to prevent the opposite bunching tendency of bosons, which causes them to seem clumped together. Using the Hanbury-Brown and Twiss (HBT) interferometer, antibunching measurement is carried out. The HBT set-up provides information about the second-order autocorrelation function, $g^2(\tau)$. Photon purity is determined by their $g^2(\tau)$ values. For quantum photonic applications, purity is one of the essential properties.

If the $g^2(\tau)$ values are smaller than 0.5, this indicates the quantum nature of the photons. According to photon statistics antibunched light is correspond to sub-Poissonian statistics. In the HBT interferometer setup, there are two single-photon detectors and a 50:50 beam splitter (BS). One of the single-photon detectors is connected to the start input of the timer and the other one is connected to the stop input.

First, the light goes through the cut-off filter and hit the beam splitter. Incident photons are divided into two paths and sent to the single-photon detectors. If the light source emits a single photon at a time after the beam splitter either hit the one detector and trigger the start input or hit the other detector and trigger the stop input. The timer counts the coincidence and produces information about the $g^2(\tau)$ function and the $g^2(\tau)$ plot is formed and shown on the computer screen as illustrated in figure 3.7. We do not expect any coincidence if one photon is emitted at a time. Therefore, in theory, we expect $g^2(\tau)$ values to be equal to zero. However, when we perform experiments we do not observe perfect antibunching due to scattered light and dark counts. Thus, if we observe $g^2(\tau) = 0.5$, we can say that our emitters demonstrate quantum characterization.[125]

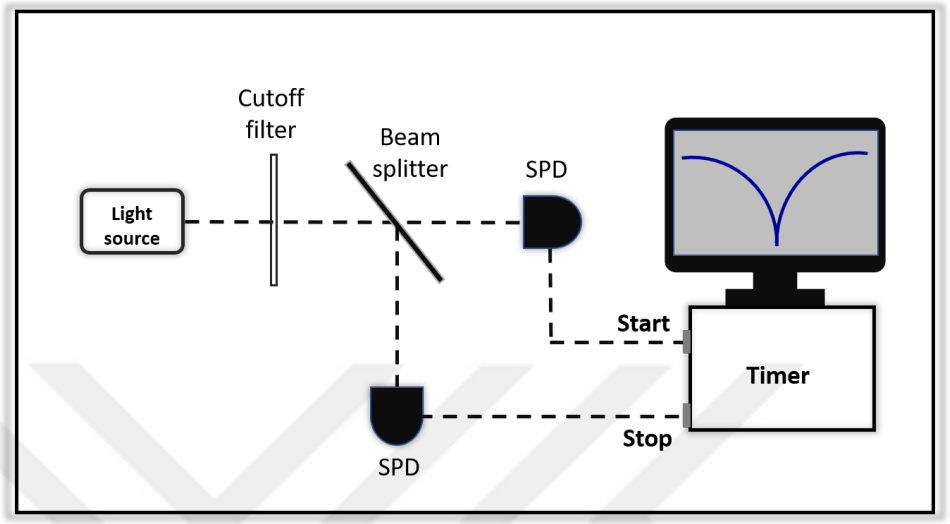


Figure 3.7: Hanbury Brown and Twiss interferometer set-up.

To confirm the quantum nature of the emitted light in h-BN flakes, we conducted antibunching experiments both under 532 nm CW and pulsed laser excitations by using the HBT interferometer. First, we excited the emitter, and emitted PL signal was collected via single mode fiber. We sent the collected PL signal directly to the HBT setup. Light is hit the beam splitter and toward the single photon detectors. Half of the photons were sent to one of the detectors and triggered the start input. The other half triggered the stop input. The timer (HydraHarp 400) measured the coincidence of the photons and recorded the data. On the screen (for CW laser excitation), the $g^2(\tau)$ function gradually takes shape.

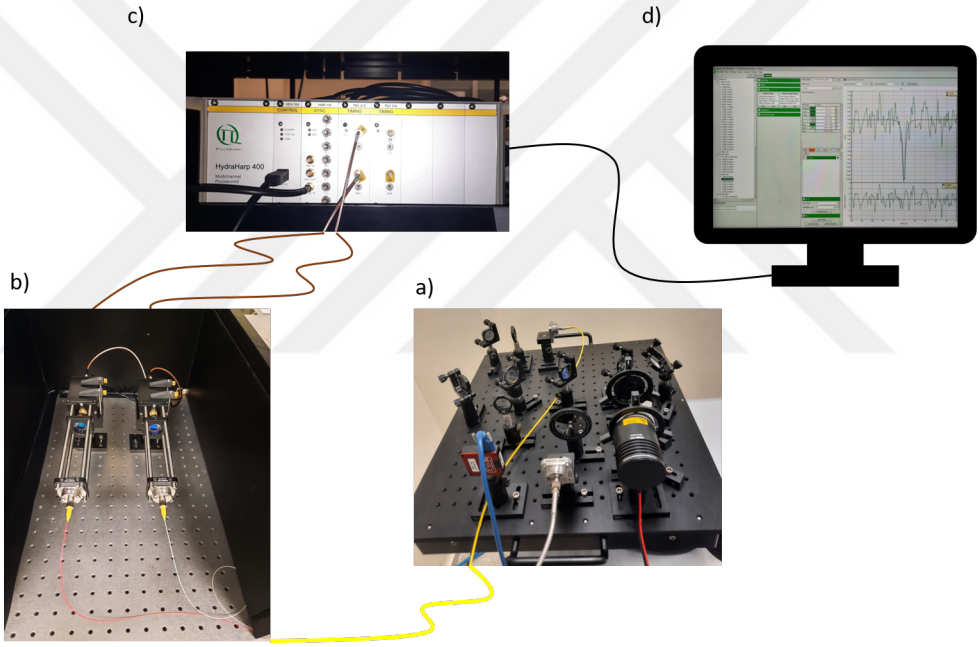


Figure 3.8: Photos of the equipment that we used in antibunching experiments a) Optical breadboard added on the cryostat. The sample is excited and emitted light is collected via single mode fiber and sent to the beam splitter where light is split. b) BS is connected to the single-photon detectors. c) The timer measures the coincidence and records the data, as a result, we obtain a $g^2(\tau)$plot as shown on the screen.

# Chapter 4

# Results

## 4.1 Optical characterization at room temperature

As we see in figure 4.1, drop-cast h-BN flakes onto the substrate that have different sizes and shapes. We also measured the Raman spectrum of the h-BN flakes. Raman spectroscopy gives us information about the chemical structure, phase, and crystallinity of the materials. The basic working principle of Raman spectroscopy is to study the inelastic scattering of light. In the materials, molecules are vibrating, thus there are vibrational modes. When light interacts with those vibrational modes light is scattered, hence the frequency of the incident light is shifted up or down, called anti-Stokes or Stokes shifts. Changes in the frequency of the incident light allow us to analyze the characteristic properties of the materials. This frequency change occurs due to energy transfer between vibrating molecules and incident light. As a result of each molecule having its molecular vibrational mode, the Raman spectrum will show peaks that are unique to each molecule. Wavenumbers (1/cm) are the standard unit of measurement for Raman frequency shifts. [126]

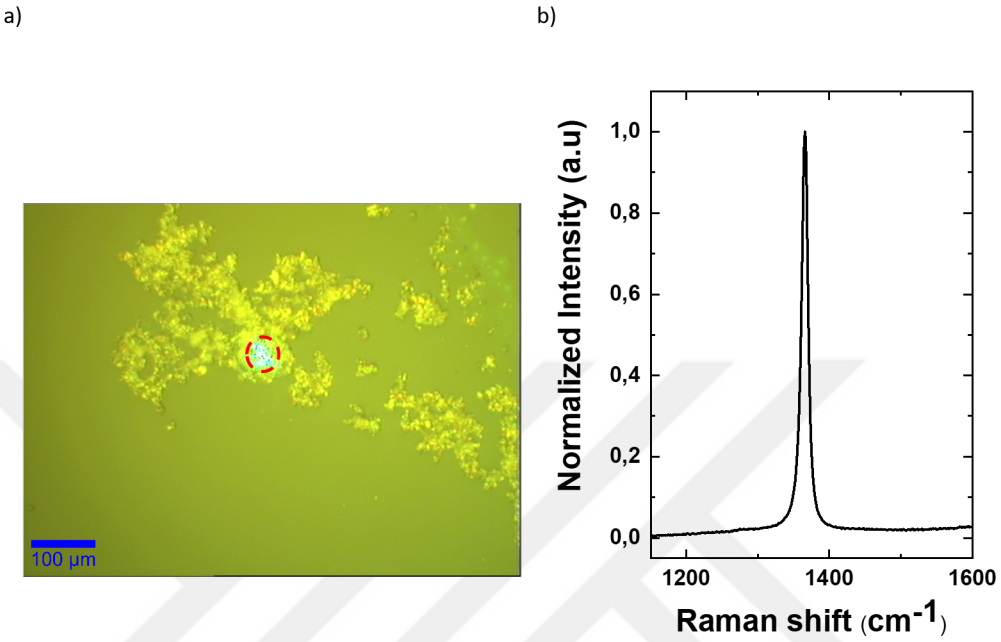


Figure 4.1: a) Optic image of drop-cast h-BN onto SiO2/Si substrate. b) Raman spectrum (1365.80 1/cm) of h-BN sample taken from red dashed circle.

To obtain the Raman spectrum of h-BN flakes, we used the Raman Confocal Microscope setup as we used for PL measurements by simply changing the configuration. When light and matter interact, light can be absorbed and scattered. After this interaction, we collect the emitted and scattered light and sent it to the spectrograph to obtain Raman and PL spectrum. Due to the inelastic scattering of the incident light, we observe a Raman peak located at 1365.80 1/cm.

Some of the example PL emissions from different defect centers were shown in figure 4.2. PL signals of defect emitters consist of a pronounced zero phonon line (ZPL) and a low-energy phonon sideband (PSB). As it was shown in the previous studies, we also observed PL emissions at different wavelenght range. After completing the optical characterizations at room temperature, we performed low-temperature measurements by using the home-built micro-PL setup.

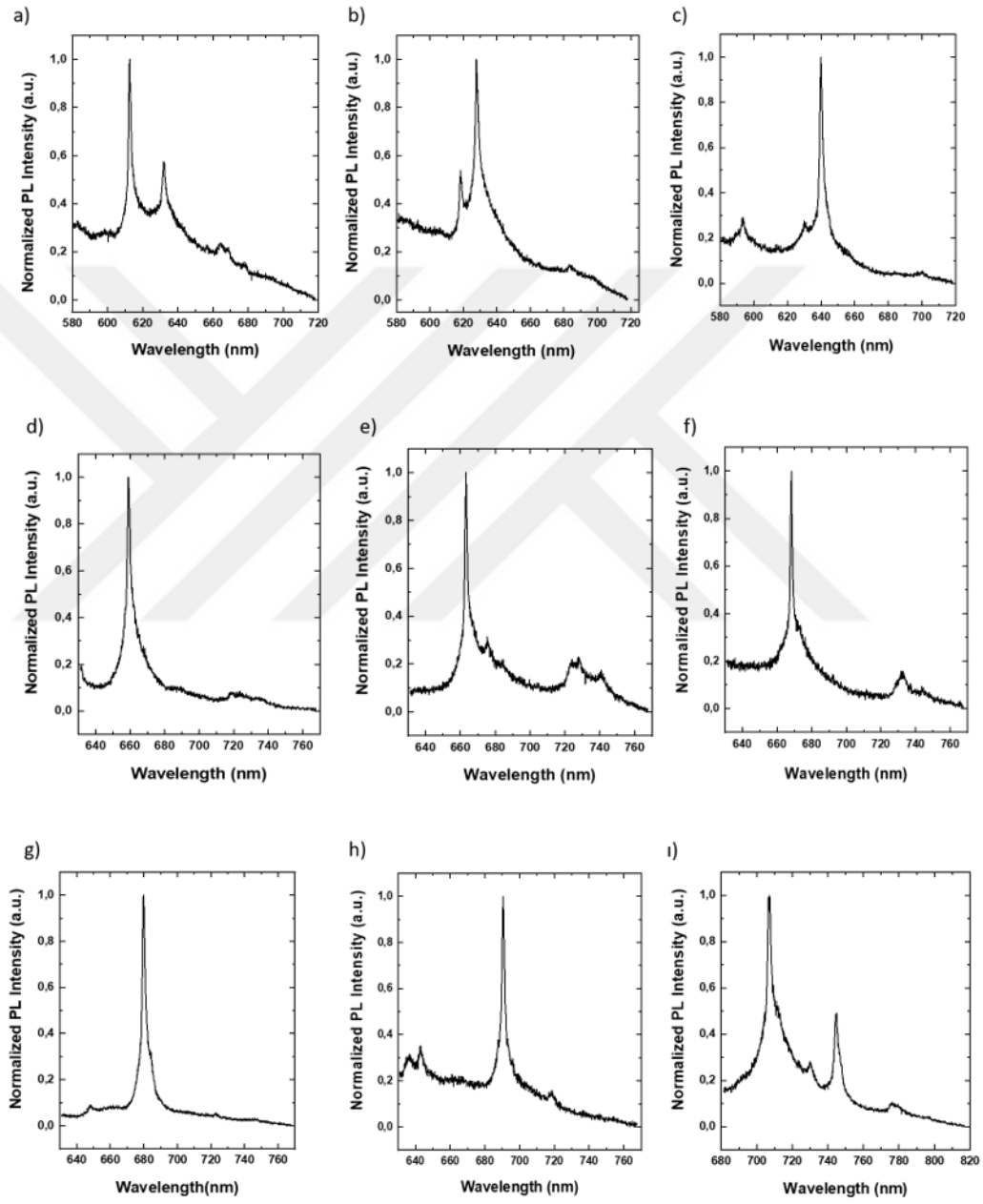


Figure 4.2: Photoluminescence spectrum of h-BN flakes. Each figure shows the PL signal located at different wavelengths which were taken from different defect centers from different samples and different h-BN flakes. 532 nm CW laser was used for the excitation process. PL signals were taken at room temperature, laser power is 600 µW.

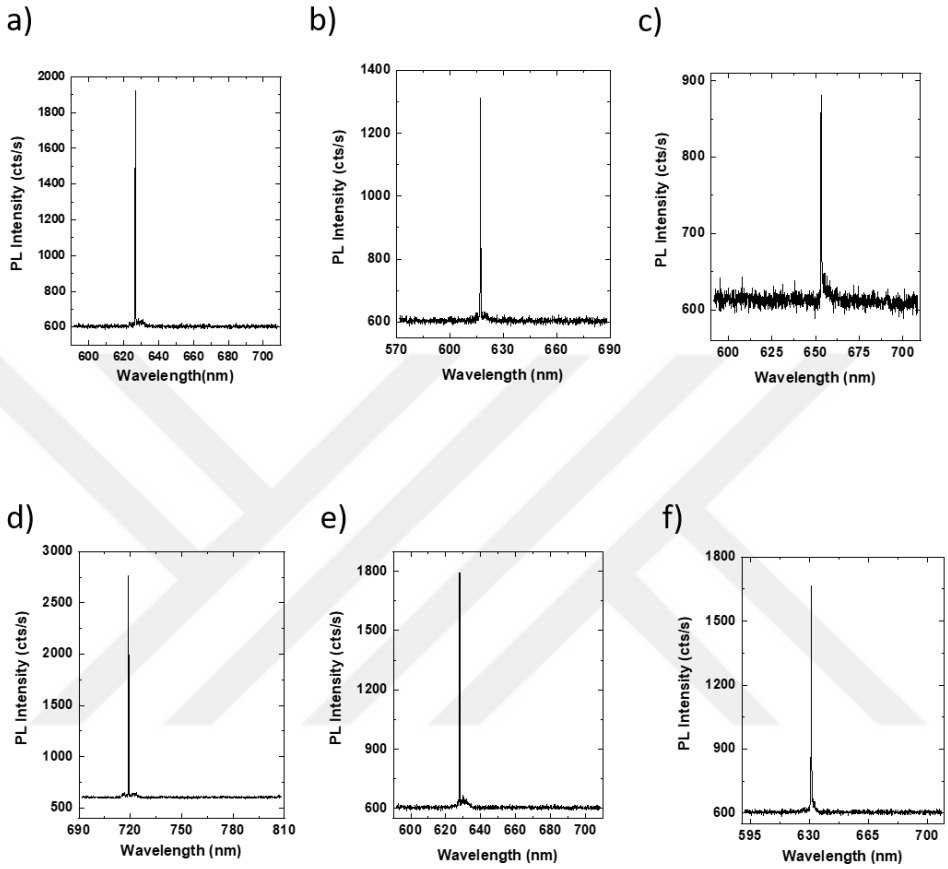


Figure 4.3: Photoluminescence spectrum of defect emitters from different h-BN flakes. All PL spectrum of defect emitters were taken at 3.5 K and for excitation, we used CW 532 nm laser, P = 100 µW. We used a 633 nm filter for (a), (e), and (f), 620 nm bandpass for (b), 650 nm bandpass for (c), and 720 nm bandpass for (d).

## 4.2 PL and spectral diffusion measurements at low temperature

We observed emission PL of defect emitters at different wavelengths. Since we worked at a low temperature, we reduced the phonon contribution to the line-shape, hence we observed a narrow, sharp PL signal. Figure 5.7 shows some of the PL emissions taken from different h-BN flakes.

Spectral diffusion causes inhomogeneous broadening which affects the photostability and preventing to obtain indistinguishable photon, which is essential for both optoelectronic and quantum photonics applications. Charge fluctuations around the local environment of the emitters cause sudden jumps in the emission wavelength over time. As a result, the linewidth of the emission spectrum is broadened.

Most of the single-photon emitters suffer from spectral diffusion. Therefore. To study the emission dynamics of defect emitters in h-BN flakes we performed spectral diffusion measurements and blinking measurements. We sent the PL signal to the CCD camera and recorded the time evolution of the emission with a time resolution of on the order of 100 ms. Some of the spectral diffusion measurements were shown in figure 5.8 For most of the emitters that we studied, we did not observe any pronounced spectral diffusion. In addition to spectral diffusion (fluctuation in the emission wavelength), emitters also suffer from blinking which is an intensity fluctuation. After we completed PL emission and spectral diffusion measurements, we sent the collected light directly to one of the Single Photon Avalanche Diodes (SPAD) with a photon timing resolution of 50 ps, thus, we enhanced the resolution of measurements from 100 ms to 1 ms. We observed very stable PL emission even at a 1 ms time scale.

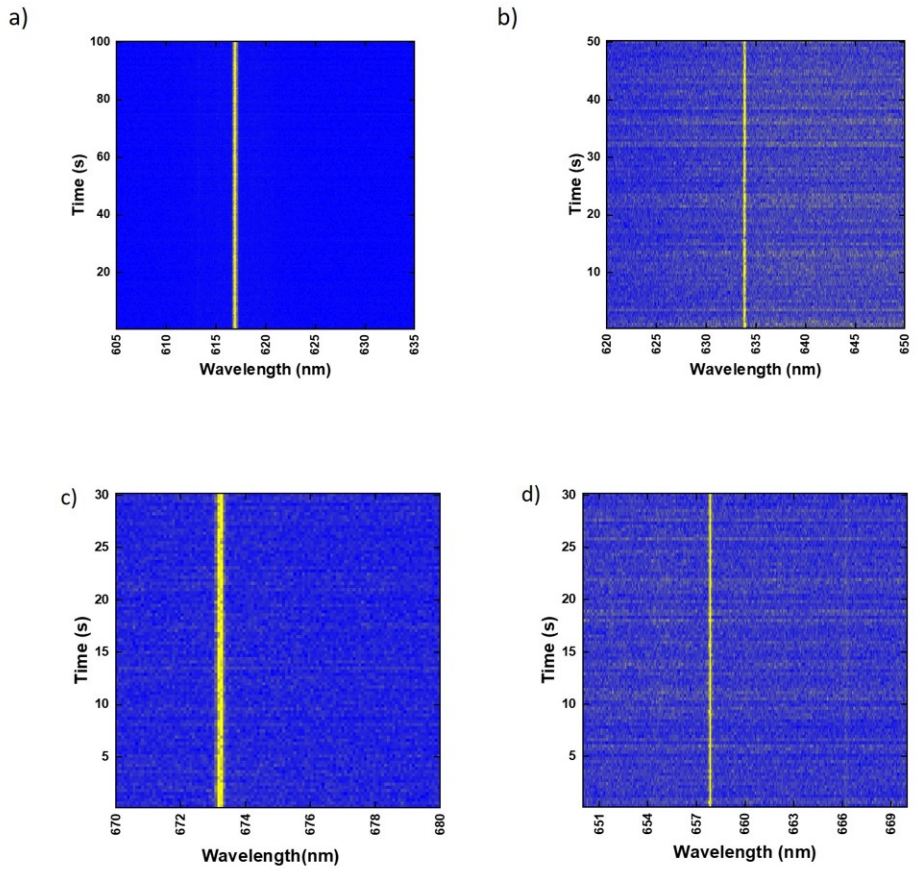


Figure 4.4: Spectral diffusion measurement results for different emitters from different flakes. The time trajectories were taken by continuously integrating. Integration time for (a) and (b) is 0.5 s, and for (c) and (d) is 0.3 s.

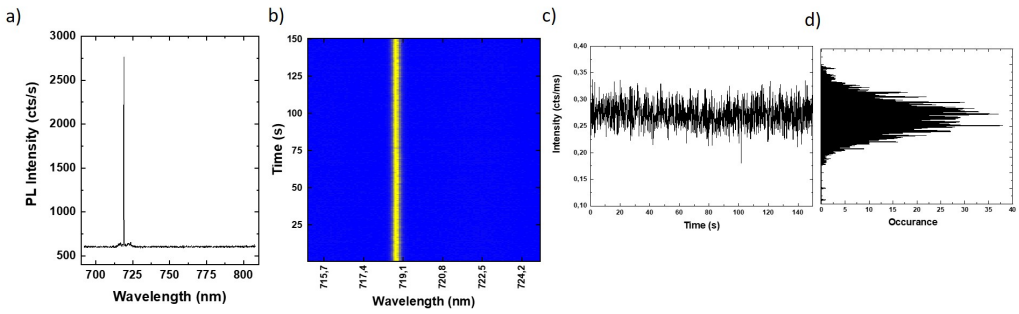


Figure 4.5: Photoluminescence of one of the emitters and spectral diffusion and blinking measurements for the same emitter. PL signal of the emitter is shown in (a), taken by using the 720 nm bandpass filter. After the photoluminescence emission was taken, we recorded the time evolution of the same emitter (a) with 0.5 s integration time, and (b) shows the spectral diffusion measurement. After that, we sent the PL signal to a single photon avalanche detector and probe the blinking, as shown (c). d) Shows the occurrence state.

We seldomly observed spectral diffusion and blinking (not shown) in the PL emission of those emitters.

## 4.3 Lifetime measurement results

We see the experimental results of lifetime measurements for different emitters in h-BN in figure 4.6. According to our research, the emitter's lifetimes are on the order of nanoseconds, which is consistent with the previous studies.

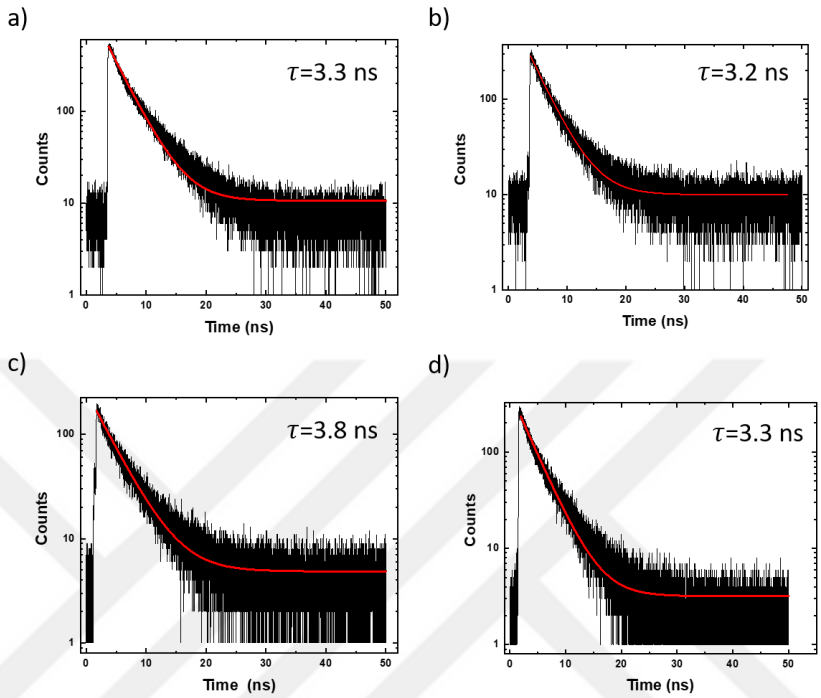


Figure 4.6: TCSPC results. The lifetime of the excited states of different defect PL emissions in h-BN flakes. 20MHz repetition is set for each measurement.

## 4.4 Antibunching results

To fit our data, we utilized the following equation

$$g^2(\tau) = \frac{1 - [1 + a + b]\ exp\left(\frac{-|\tau|}{\tau_1}\right) + a\ exp\ \left(\frac{-|\tau|}{\tau_2}\right) + b + bkgr - 1}{bkgr}, \qquad (4.1)$$

where a and b are background, bkgr background by uncorrelated light and $\tau_1$ (lifetime of excited state) and $\tau_2$ (lifetime of meta-stable state) are antibunching constants, and t is the delay time. Figure 4.7 shows the photon antibunching measurement results for two different emitters under CW and pulsed laser excitation. For different emitters, the $g^2(0)$ values that we obtain vary from 0.29 to 0.40. Thus, the photon antibunching experience confirms the quantum nature of those emitters in h-BN.

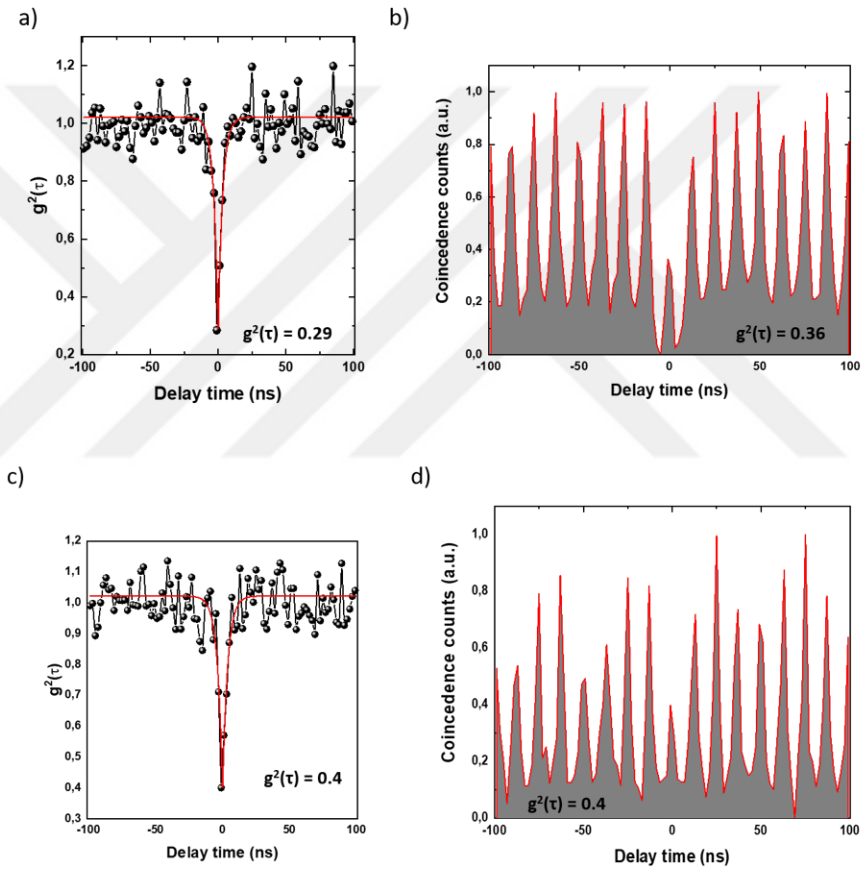


Figure 4.7: Photon antibunching measurements. a) and b) show antibunching results for the same emitter under CW and pulsed laser excitation, respectively. c) and d) show antibunching results for another emitter under CW and pulsed laser excitation. For both emitters, $g^2(\tau)$ values at zero delay time are smaller than 0.5, which confirms the quantum nature of those emitters.

# Chapter 5

# Controlling the PL of quantum emitters in h-BN via an external magnetic field

There are magnets mounted in a cryostat that we used for low-temperature measurements. To study PL emission under applied magnetic field, we used our home-built micro-PL setup that shown in chapter. We observed photo darkening effect when we applied external out-of-plane magnetic field.

## 5.1 Magneto-PL studies at low temperature

After showing the existence of the stable quantum light emitters in h-BN, we finally investigated PL emissions under an applied external magnetic field. Despite the fact that early magneto-photoluminescence (PL) research showed nonmagnetic behavior [40], recent magneto-PL experiment 41 as well as optically detected magnetic resonance (ODMR) experiments [42, 127, 128] showed spin defects in h-BN. We investigated the PL emission dynamics of single-photon emitters in h-BN under an applied out-of-plane external magnetic field at cryogenic temperature.

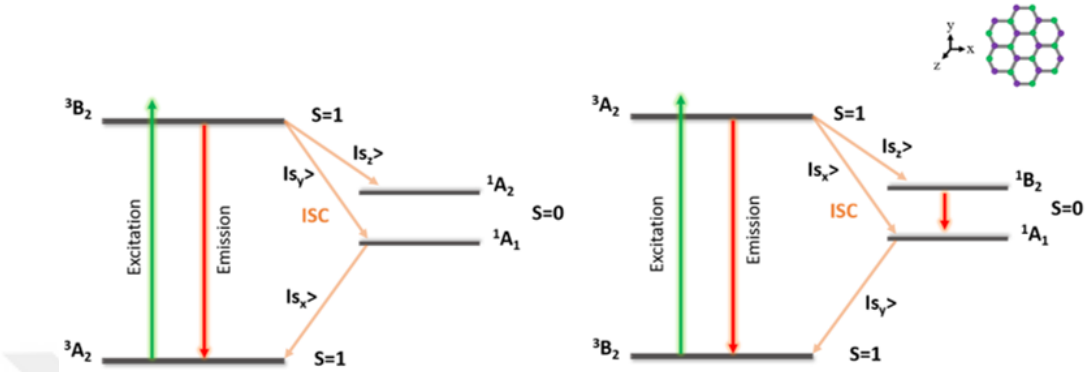


Figure 5.1: Diagram of the electronic structure including the triplet excited states ($^3B_2$, $^3A_2$), triplet ground state ($^3A_2$, $^3B_2$), and singlet metastable states ($1A^2$, $^1A_1$, and $^1B_2$). The vertical green arrow indicates the optical excitation, the red arrow represents to radiative transition, and orange arrow corresponds to spin selective non-radiative intersystem crossing (ISC) transitions. $|Sx>$, $|Sy>$, and $|Sz>$ are zero-field spin eigenstates in triplet configuration.

We observed that the PL intensity of emitters showed magnetic field dependence and decreased with the increased magnetic field. Exarhos et. al., by utilizing the molecular orbital theory and group theory calculation, they explained the behavior of the PL intensity change with respect to applied in-plane and out-of-plane magnetic fields.

We obtained the two electronic level diagrams, which are illustrated in figure 5.16, from reference 41 to explain the PL intensity decrease seen during our experiments under the applied out-of-plane (z-direction) magnetic field.Spin multiplicity and intersystem crossing (ISC) are briefly discussed in chapter 4. The intersystem crossing is the non-radiative transition from triplet (S=1) to singlet (S=0) state or a singlet to triplet where spin of the electron flips. The PL simulations of those configurations performed in reference 41, and they predicted that PL intensity should reach its maximum value at B=0 and decrease with the applied out-of-plane magnetic field if ISC crossing occurs from triplet state to metastable state and from metastable state to triplet ground state through the lowest-lying single state $^1A_1$. PL intensity decrease with the applied out-of-plane magnetic field when the final ISC emerges from the lowest state.

We looked at how steady PL emissions behaved when an out-of-plane magnetic field was added. The low-temperature PL emission spectra of four distinct emitters (E) with (red curve) and without (black curve) applied external magnetic fields are displayed in the top panel of figure 5.2. Six distinct emitters were examined, and four of them had considerable magnetic field dependence.Six distinct emitters were examined, and four of them had considerable magnetic field dependence. Only one of the emitters (E6) was not sensitive to the applied magnetic field, shown in figure 5.3. We increased the PL intensity each time by altering the emitter location with an x, y, and z nanopositioner in order to rule out the drift-related PL drop under applied magnetic fields. We also noticed that the process is reversible, which means that when the applied field is removed, the PL intensity nearly returns to its zero-field value. To show the reversibility of the process, we took the PL spectrum of the each emitter after applied magnetic filed is removed. The bottom panel of the figure 5.2 shows zero-field PL spectra of the each emitter. In terms of PL intensity, emitter 6 showed no discernible change.

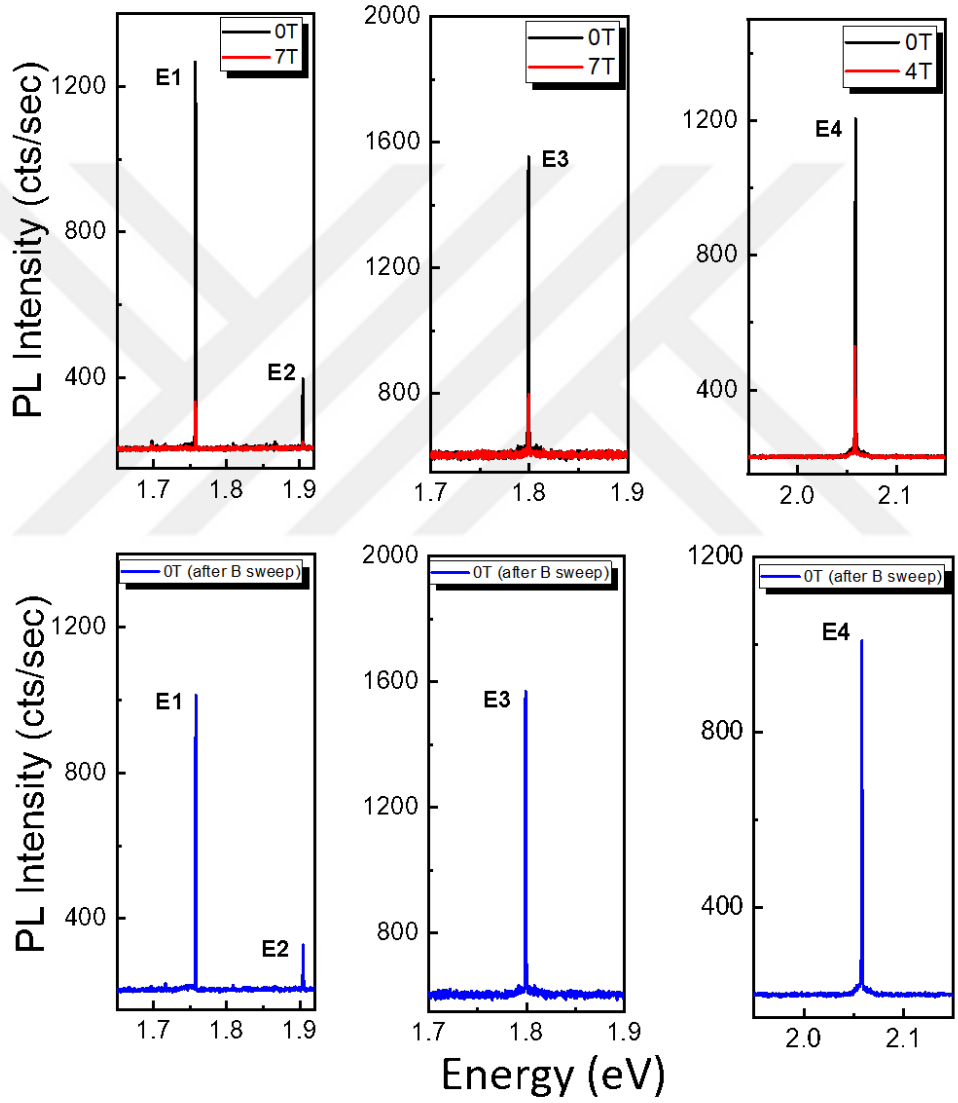


Figure 5.2: Top panel shows the PL spectra of four different emitters (E1, E2, E3, and E4) with (red color), and without (black color) applied external out-of-plane magnetic field. The bottom panel shows PL spectra of the same emitters after the magnetic field is removed.

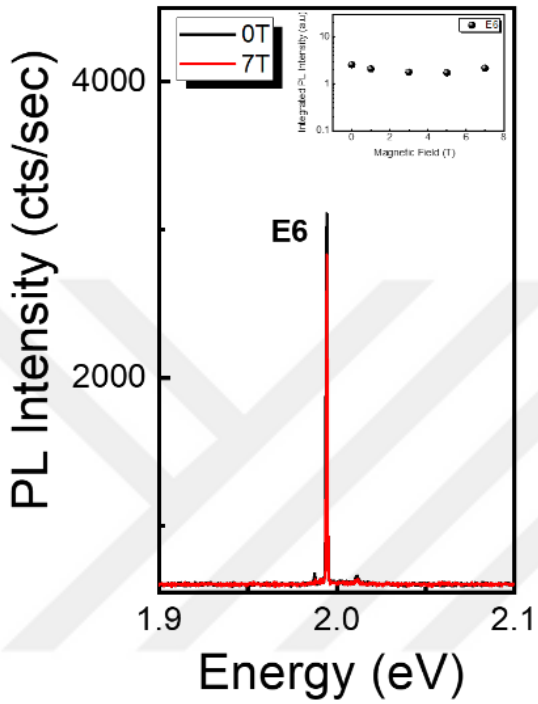


Figure 5.3: PL spectrum of the emitter (E6) with (red color) and without (black color) applied magnetic field. Inset graph shows the integrated PL intensity of the same flake as a function the applied magnetic field.

Similar to earlier experimental studies, we found no significant Zeeman splitting or wavelength shifting of the ZPL emission. In figure 5.5, we plot the integrated PL intensity of each emitter at various magnetic fields to further highlight the significant impact of the applied magnetic field on the PL emission. Strong magnetic field dependence can be seen in the integrated PL intensity, which also decreases as magnetic fields are increased. Once the field is increased from 0T to 7T, the E1 and E2's PL intensity decreases by an order of magnitude.

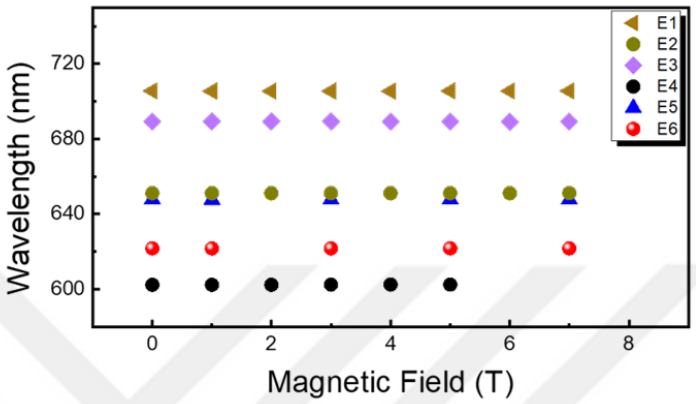


Figure 5.4: ZPL peak positions of h-BN emitters versus applied out-of-plane magnetic field.

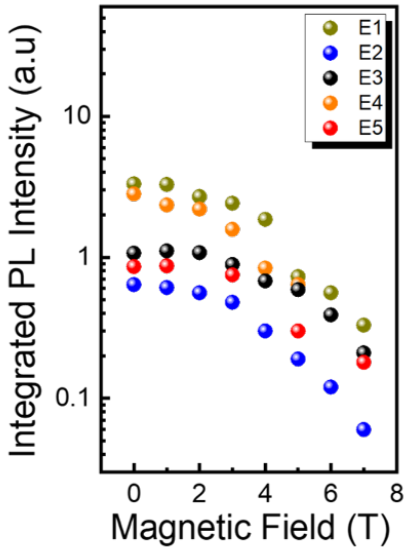


Figure 5.5: Integrated PL intensity of five h-BN defect emitters as a function of the applied out-of-plane magnetic field. By fitting the PL spectra of each emitter with the Lorentzian function, the area under the PL spectrum is taken as integrated PL intensity.

# Chapter 6

# Conclusion

In chapter 1, we discussed some of the quantum technologies such as quantum computing, quantum sensing, and quantum key distribution, what makes them different from current counterparts, why we need them, and what are the advantages. We also discussed some of the materials that are hosting quantum emitters, including color centers in diamond, carbon nanotubes, transition metal dichalcogenides, and their possible quantum applications.

In chapter 2, we covered some of the highlighted developments in science through the years that lead us to this study. We discussed photon properties, photon absorption, and the emission by spontaneous and stimulated emission. We discussed antibunched light and chractericaton of photons. We discussed the structure, electronic and optical properties of h-BN and single-photon generation in h-BN.

In chapter 3, we discussed sample preparation and experimental measuring systems. We drop-casted h-BN solution onto $SiO_2/Si$ substrate and let it dry over a night. The next day we annealed the sample for 30 minutes at 850 °C under 1 Torr argon pressure. To check whether we created optically active defect centers or not we used Raman Confocal Microscope, and we performed room temperature optical characterization.

To study photostability of emitters we performed PL, SD, and blinking measurements at low temperature. To do that, we constructed micro-PL setup. We showed the equipments that we used during the PL and SD measurements. To study photodynamic of emitters, we measured the lifetimes of excited states by using time-correlated single-photon counting method (TCSPC. We discussed the (TCSPC) method and how histogram plot is formed during the measurments. We also studied the quantum nature of the emitter, for that we constructed HBT interferometer. We discussed how we performed antibunching measurements.

In chapter 4, we showed the results and discussed. First we confirmed that we created optically active defect centers via thermal annealing by performing the optical characterizations at room temperature with Raman Confocal Microscope. We found PL emission from different defect centers at various emission wavelength. We showed photostable emitters in h-BN. Our lifetime measurement results are on the order of few nanoseconds which agrees the previous studies. The antibunching results also indicated the quantum nature of those emitters.

In chapter 5, we performed magneto-PL measurements and we controlled the PL emission of emitters in h-BN by applying external out-of plane magnetic field. We observed photo-darkening effect and magnetic field dependence in the terms of PL emission. We observed that PL intensities of emitters decreased when we applied magnetic field in the Faraday geometry. Another interesting thing that we observed is this process is reversible which means that when we remove the applied magnetic field PL intensities returned almost initial PL intensities.

# Bibliography


[1] I. Aharonovich, D. Englund, and M. Toth, "Solid-state single-photon emitters," *Nature Photonics*, vol. 10, no. 10, pp. 631–641, 2016.

[2] H. S. Zhong, H. Wang, Y. H. Deng, M. C. Chen, L. C. Peng, Y. H. Luo, J. Qin, D. Wu, X. Ding, Y. Hu, P. Hu, X. Y. Yang, W. J. Zhang, H. Li, Y. Li, X. Jiang, L. Gan, G. Yang, L. You, Z. Wang, L. Li, N. L. Liu, C. Y. Lu, and J. W. Pan, "Quantum computational advantage using photons," *Science*, vol. 370, no. 6523, pp. 1460–1463, 2020.

[3] "Single-photon quantum imaging via single-photon illumination," *Applied Physics Letters*, vol. 117, no. 21, 2020.

[4] B. J. Lawrie, C. E. Marvinney, Y. Y. Pai, M. A. Feldman, J. Zhang, A. J. Miller, C. Hua, E. Dumitrescu, and G. B. Halász, "Multifunctional Superconducting Nanowire Quantum Sensors," *Physical Review Applied*, vol. 16, no. 6, p. 1, 2021.

[5] C. Y. Lu and J. W. Pan, "Quantum-dot single-photon sources for the quantum internet," *Nature Nanotechnology*, vol. 16, no. 12, pp. 1294–1296, 2021.

[6] J. Wang, F. Sciarrino, A. Laing, and M. G. Thompson, "Integrated photonic quantum technologies," *Nature Photonics*, vol. 14, no. 5, pp. 273–284, 2020.

[7] D. Bonneau, E. Engin, K. Ohira, N. Suzuki, H. Yoshida, N. Iizuka, M. Ezaki, C. M. Natarajan, M. G. Tanner, R. H. Hadfield, S. N. Dorenbos, V. Zwiller, J. L. O'Brien, and M. G. Thompson, "Quantum interference and manipulation of entanglement in silicon wire waveguide quantum circuits," *New Journal of Physics*, vol. 14, 2012.

[8] A. Acín, I. Bloch, H. Buhrman, T. Calarco, C. Eichler, J. Eisert, D. Esteve, N. Gisin, S. J. Glaser, F. Jelezko, S. Kuhr, M. Lewenstein, M. F. Riedel, P. O. Schmidt, R. Thew, A. Wallraff, I. Walmsley, and F. K. Wilhelm, "The quantum technologies roadmap: A European community view," *New Journal of Physics*, vol. 20, no. 8, 2018.

[9] E. Knill, "Q  A Quantum computing," vol. 463, no. January, 2010.

[10] C. Ugwuishiwu and O. Ugochukwu, "An overview of Quantum Cryptography and Shor's Algorithm," *International Journal of Advanced Trends in Computer Science and Engineering*, vol. 9, no. 5, pp. 7487–7495, 2020.

[11] Z.-C. Duan, J.-P. Li, J. Qin, Y. Yu, Y.-H. Huo, S. Höfling, C.-Y. Lu, N.-L. Liu, K. Chen, and J.-W. Pan, "Proof-of-principle demonstration of compiled Shor's algorithm using a quantum dot single-photon source," *Optics Express*, vol. 28, no. 13, p. 18917, 2020.

[12] G. Frascella, S. Agne, F. Y. Khalili, and M. V. Chekhova, "Overcoming detection loss and noise in squeezing-based optical sensing," *npj Quantum Information*, vol. 7, no. 1, pp. 2–7, 2021.

[13] C. D. Marciniak, T. Feldker, I. Pogorelov, R. Kaubruegger, D. V. Vasilyev, R. van Bijnen, P. Schindler, P. Zoller, R. Blatt, and T. Monz, "Optimal metrology with programmable quantum sensors," *Nature*, vol. 603, no. 7902, pp. 604–609, 2022.

[14] S. Wang, Z. Q. Yin, D. Y. He, W. Chen, R. Q. Wang, P. Ye, Y. Zhou, G. J. Fan-Yuan, F. X. Wang, W. Chen, Y. G. Zhu, P. V. Morozov, A. V. Divochiy, Z. Zhou, G. C. Guo, and Z. F. Han, "Twin-field quantum key distribution over 830-km fibre," *Nature Photonics*, vol. 16, no. 2, pp. 154–161, 2022.

[15] M. Anderson, T. Müller, J. Skiba-Szymanska, A. B. Krysa, J. Huwer, R. M. Stevenson, J. Heffernan, D. A. Ritchie, and A. J. Shields, "Coherence in single photon emission from droplet epitaxy and Stranski-Krastanov quantum dots in the telecom C-band," *Applied Physics Letters*, vol. 118, no. 1, 2021.

[16] J. Zaumseil, "Luminescent Defects in Single-Walled Carbon Nanotubes for Applications," *Advanced Optical Materials*, vol. 10, no. 2, 2022.

[17] A. Lohrmann, S. Pezzagna, I. Dobrinets, P. Spinicelli, V. Jacques, J. F. Roch, J. Meijer, and A. M. Zaitsev, "Diamond based light-emitting diode for visible single-photon emission at room temperature," *Applied Physics Letters*, vol. 99, no. 25, 2011.

[18] K. Parto, S. I. Azzam, K. Banerjee, and G. Moody, "Defect and strain engineering of monolayer WSe2 enables site-controlled single-photon emission up to 150 K," *Nature Communications*, vol. 12, no. 1, pp. 1–8, 2021.

[19] N. Mendelson, D. Chugh, J. R. Reimers, T. S. Cheng, A. Gottscholl, H. Long, C. J. Mellor, A. Zettl, V. Dyakonov, P. H. Beton, S. V. Novikov, C. Jagadish, H. H. Tan, M. J. Ford, M. Toth, C. Bradac, and I. Aharonovich, "Identifying carbon as the source of visible single-photon emission from hexagonal boron nitride," *Nature Materials*, vol. 20, no. 3, pp. 321–328, 2021.

[20] A. Sajid, M. J. Ford, and J. R. Reimers, "Single-photon emitters in hexagonal boron nitride: a review of progress," *Reports on Progress in Physics*, vol. 83, no. 4, 2020.

[21] M. D. Eisaman, J. Fan, A. Migdall, and S. V. Polyakov, "Invited Review Article: Single-photon sources and detectors," *Review of Scientific Instruments*, vol. 82, no. 7, 2011.

[22] E. Wu, J. R. Rabeau, G. Roger, F. Treussart, H. Zeng, P. Grangier, S. Prawer, and J. F. Roch, "Room temperature triggered single-photon source in the near infrared," *New Journal of Physics*, vol. 9, 2007.

[23] J. T. Choy, B. J. Hausmann, T. M. Babinec, I. Bulu, M. Khan, P. Maletinsky, A. Yacoby, and M. Loňar, "Enhanced single-photon emission from a diamond-Silver aperture," *Nature Photonics*, vol. 5, no. 12, pp. 738–743, 2011.

[24] M. Ruf, N. H. Wan, H. Choi, D. Englund, and R. Hanson, "Quantum networks based on color centers in diamond," *Journal of Applied Physics*, vol. 130, no. 7, 2021.

[25] S. Kolatschek, C. Nawrath, S. Bauer, J. Huang, J. Fischer, R. Sittig, M. Jetter, S. L. Portalupi, and P. Michler, "Bright Purcell Enhanced Single-Photon Source in the Telecom O-Band Based on a Quantum Dot in a Circular Bragg Grating," *Nano Letters*, 2021.

[26] P. Holewa, A. Sakanas, U. M. Gür, P. Mrowiński, A. Huck, B.-Y. Wang, A. Musiał, K. Yvind, N. Gregersen, M. Syperek, and E. Semenova, "Bright Quantum Dot Single-Photon Emitters at Telecom Bands Heterogeneously Integrated on Si," *ACS Photonics*, 2022.

[27] Y. Lu, A. Bengtsson, J. J. Burnett, B. Suri, S. R. Sathyamoorthy, H. R. Nilsson, M. Scigliuzzo, J. Bylander, G. Johansson, and P. Delsing, "Quantum efficiency, purity and stability of a tunable, narrowband microwave single-photon source," *npj Quantum Information*, vol. 7, no. 1, 2021.

[28] X. He, N. F. Hartmann, X. Ma, Y. Kim, R. Ihly, J. L. Blackburn, W. Gao, J. Kono, Y. Yomogida, A. Hirano, T. Tanaka, H. Kataura, H. Htoon, and S. K. Doorn, "Tunable room-Temperature single-photon emission at telecom wavelengths from sp 3 defects in carbon nanotubes," *Nature Photonics*, vol. 11, no. 9, pp. 577–582, 2017.

[29] A. Ishii, X. He, N. F. Hartmann, H. Machiya, H. Htoon, S. K. Doorn, and Y. K. Kato, "Enhanced Single-Photon Emission from Carbon-Nanotube Dopant States Coupled to Silicon Microcavities," *Nano Letters*, vol. 18, no. 6, pp. 3873–3878, 2018.

[30] K. F. Mak and J. Shan, "Photonics and optoelectronics of 2D semiconductor transition metal dichalcogenides," *Nature Photonics*, vol. 10, no. 4, pp. 216–226, 2016.

[31] M. Toth and I. Aharonovich, "Single Photon Sources in Atomically Thin Materials," *Annual Review of Physical Chemistry*, vol. 70, pp. 123–142, 2019.

[32] W. Wang and X. Ma, "Strain-Induced Trapping of Indirect Excitons in MoSe2/WSe2Heterostructures," *ACS Photonics*, vol. 7, no. 9, pp. 2460–2467, 2020.

[33] P. Rivera, H. Yu, K. L. Seyler, N. P. Wilson, W. Yao, and X. Xu, "Interlayer valley excitons in heterobilayers of transition metal dichalcogenides," *Nature Nanotechnology*, vol. 13, no. 11, pp. 1004–1015, 2018.

[34] C. Li, N. Mendelson, R. Ritika, Y. Chen, Z. Q. Xu, M. Toth, and I. Aharonovich, "Scalable and Deterministic Fabrication of Quantum Emitter Arrays from Hexagonal Boron Nitride," *Nano Letters*, vol. 21, no. 8, pp. 3626–3632, 2021.

[35] J. D. Caldwell, I. Aharonovich, G. Cassabois, J. H. Edgar, B. Gil, and D. N. Basov, "Photonics with hexagonal boron nitride," *Nature Reviews Materials*, vol. 4, no. 8, pp. 552–567, 2019.

[36] B. Shevitski, S. M. Gilbert, C. T. Chen, C. Kastl, E. S. Barnard, E. Wong, D. F. Ogletree, K. Watanabe, T. Taniguchi, A. Zettl, and S. Aloni, "Blue-light-emitting color centers in high-quality hexagonal boron nitride," *Physical Review B*, vol. 100, no. 15, p. 155419, 2019.

[37] Y. Xia, Q. Li, J. Kim, W. Bao, C. Gong, S. Yang, Y. Wang, and X. Zhang, "Room-Temperature Giant Stark Effect of Single Photon Emitter in van der Waals Material," *Nano Letters*, vol. 19, no. 10, pp. 7100–7105, 2019.

[38] Y. Chen, C. Li, S. White, M. Nonahal, Z. Q. Xu, K. Watanabe, T. Taniguchi, M. Toth, T. T. Tran, and I. Aharonovich, "Generation of High-Density Quantum Emitters in High-Quality, Exfoliated Hexagonal Boron Nitride," *ACS Applied Materials and Interfaces*, vol. 13, no. 39, pp. 47283–47292, 2021.

[39] Q.-H. Tan, J.-M. Lai, X.-L. Liu, Y.-Z. Xue, X.-M. Dou, B.-Q. Sun, W.-B. Gao, P.-H. Tan, and J. Zhang, "Robust Ultraviolet to Near-infrared Quantum Emitters in Hexagonal Boron Nitride up to 1100 K," pp. 1–9, 2019.

[40] X. Li, G. D. Shepard, A. Cupo, N. Camporeale, K. Shayan, Y. Luo, V. Meunier, and S. Strauf, "Nonmagnetic Quantum Emitters in Boron Nitride with Ultranarrow and Sideband-Free Emission Spectra," *ACS Nano*, vol. 11, no. 7, pp. 6652–6660, 2017.

[41] A. L. Exarhos, D. A. Hopper, R. N. Patel, M. W. Doherty, and L. C. Bassett, "Magnetic-field-dependent quantum emission in hexagonal boron nitride at room temperature," *Nature Communications*, vol. 10, no. 1, pp. 1–8, 2019.

[42] H. L. Stern, Q. Gu, J. Jarman, S. Eizagirre Barker, N. Mendelson, D. Chugh, S. Schott, H. H. Tan, H. Sirringhaus, I. Aharonovich, and M. Atatüre, "Room-temperature optically detected magnetic resonance of single defects in hexagonal boron nitride," *Nature Communications*, vol. 13, no. 1, pp. 1–9, 2022.

[43] M. Atatüre, D. Englund, N. Vamivakas, S. Y. Lee, and J. Wrachtrup, "Material platforms for spin-based photonic quantum technologies," *Nature Reviews Materials*, vol. 3, no. 5, pp. 38–51, 2018.

[44] D. D. Awschalom, R. Hanson, J. Wrachtrup, and B. B. Zhou, "Quantum technologies with optically interfaced solid-state spins," *Nature Photonics*, vol. 12, no. 9, pp. 516–527, 2018.

[45] M. Abdi, J. P. Chou, A. Gali, and M. B. Plenio, "Color Centers in Hexagonal Boron Nitride Monolayers: A Group Theory and Ab Initio Analysis," *ACS Photonics*, vol. 5, no. 5, pp. 1967–1976, 2018.

[46] M. A. Feldman, C. E. Marvinney, A. A. Puretzky, and B. J. Lawrie, "Evidence of photochromism in a hexagonal boron nitride single-photon emitter," *Optica*, vol. 8, no. 1, p. 1, 2021.

[47] C. Fournier, A. Plaud, S. Roux, A. Pierret, M. Rosticher, K. Watanabe, T. Taniguchi, S. Buil, X. Quélin, J. Barjon, J. P. Hermier, and A. Delteil, "Position-controlled quantum emitters with reproducible emission wavelength in hexagonal boron nitride," *Nature Communications*, vol. 12, no. 1, pp. 1–6, 2021.

[48] G. Grosso, H. Moon, B. Lienhard, S. Ali, D. K. Efetov, M. M. Furchi, P. Jarillo-Herrero, M. J. Ford, I. Aharonovich, and D. Englund, "Tunable and high-purity room temperature single-photon emission from atomic defects in hexagonal boron nitride," *Nature Communications*, vol. 8, no. 1, pp. 1–8, 2017.

[49] P. Rice, *An Introduction to Quantum Optics An open systems approach*.

[50] R. W. Boyd and S. G. Lukishova, *Quantum Photonics : Pioneering Advances and Emerging Applications*. No. February, 2019.

[51] B. Saleh and M. Teich, *Fundamentals of Photonics 3rd Edition*, vol. 5. 2013.

[52] M. Fox, *Quantum optics*, vol. 4. 2016.

[53] M. Kaur and M. Singh, "Quantum double-double-slit experiment with momentum entangled photons," *Scientific Reports*, vol. 10, no. 1, pp. 1–11, 2020.

[54] P. A. M. Dirac, "The quantum theory of the emission and absorption of radiation," 1927.

[55] T. P. Pearsall, *Quantum Photonics Graduate Texts in Physics*.

[56] J. N. Demas and S. E. Demas, *Luminescence  Origins of Luminescences*. 2014.

[57] G. Tallents, *An Introduction to the Atomic and Radiaion Physics of Plasmas*. 2018.

[58] R.J.Keyes, *The Photon Detection Process*. 1977.

[59] H. Cao, Y. Ling, J. Y. Xu, C. Q. Cao, and P. Kumar, "Photon statistics of random lasers with resonant feedback," *Physical Review Letters*, vol. 86, no. 20, 2001.

[60] G. J. M. D.F.Walls, *Quantom Optics*.

[61] W. Vogel and D. G. Welsch, *Quantum Optics: Third, revised and extended edition*. 2006.

[62] W. E. L. Marlan O. Scully, "Quantum Theory of an Optical Maser I. General Theory," 1967.

[63] A. Y. E. Hanamura, Y. Kawabe, *Quantum Nonlinear Optics*, vol. 4.

[64] H. Wang, J. Guo, J. Miao, W. Luo, Y. Gu, R. Xie, F. Wang, L. Zhang, P. Wang, and W. Hu, "Emerging Single-Photon Detectors Based on Low-Dimensional Materials," *Small*, vol. 18, no. 5, pp. 1–16, 2022.

[65] D. Renker and E. Lorenz, "Advances in solid state photon detectors," *Journal of Instrumentation*, vol. 4, no. 4, 2009.

[66] R. Loudon, "Photon Bunching and Antibunching," *Physics Bulletin*, vol. 27, no. 1, pp. 21–23, 1976.

[67] D. J. Griffiths, *Introduction to quantum mechanics*.

[68] Y. Shih, *An intrduction to Quantum Optics*, vol. 4. 2016.

[69] R. Q. T. Hanbury Brown, "I . Basic theory : the correlation between photons in coherent beams of radiation," pp. 300–324, 1957.

[70] H. J. Kimble, M. Dagenais, and L. Mandel, "Photon antibunching in resonance fluorescence," *Physical Review Letters*, vol. 39, no. 11, pp. 691–695, 1977.

[71] A. Aspect, D. Boiron, and C. Westbrook, "Quantum atom optics with bosons and fermions," *Europhysics News*, vol. 39, no. 1, pp. 25–29, 2008.

[72] S. J. F. Clauser and J. F., "Exprimental Test of Local Hidden Variable Theories," 1972.

[73] J. F. Clauser, "Experimental distinction between the quantum and classical field-theoretic predictions for the photoelectric effect," *Physical Review D*, vol. 9, no. 4, pp. 853–860, 1974.

[74] D. E. Chang, A. S. Sørensen, E. A. Demler, and M. D. Lukin, "A single-photon transistor using nanoscale surface plasmons," *Nature Physics*, vol. 3, no. 11, pp. 807–812, 2007.

[75] P. W. Shor and J. Preskill, "Simple proof of security of the BB84 quantum key distribution protocol," *Physical Review Letters*, vol. 85, no. 2, pp. 441–444, 2000.

[76] A. Lohrmann, N. Iwamoto, Z. Bodrog, S. Castelletto, T. Ohshima, T. J. Karle, A. Gali, S. Prawer, J. C. McCallum, and B. C. Johnson, "Single-photon emitting diode in silicon carbide," *Nature Communications*, vol. 6, 2015.

[77] S. Wehner, D. Elkouss, and R. Hanson, "Quantum internet: A vision for the road ahead," *Science*, vol. 362, no. 6412, 2018.

[78] K. Fukui and S. Takeda, "Building a large-scale quantum computer with continuous-variable optical technologies," *Journal of Physics B: Atomic, Molecular and Optical Physics*, vol. 55, no. 1, p. 012001, 2022.

[79] A. Gottscholl, M. Diez, V. Soltamov, C. Kasper, D. Krauße, A. Sperlich, M. Kianinia, C. Bradac, I. Aharonovich, and V. Dyakonov, "Spin defects in hBN as promising temperature, pressure and magnetic field quantum sensors," *Nature Communications*, vol. 12, no. 1, pp. 6–13, 2021.

[80] I. A. Khramtsov, A. A. Vyshnevyy, and D. Y. Fedyanin, "Enhancing the brightness of electrically driven single-photon sources using color centers in silicon carbide," *npj Quantum Information*, vol. 4, no. 1, 2018.

[81] O. Gazzano, S. Michaelis De Vasconcellos, C. Arnold, A. Nowak, E. Galopin, I. Sagnes, L. Lanco, A. Lemaître, and P. Senellart, "Bright solid-state sources of indistinguishable single photons," *Nature Communications*, vol. 4, 2013.

[82] F. Graffitti, J. Kelly-Massicotte, A. Fedrizzi, and A. M. Brańczyk, "Design considerations for high-purity heralded single-photon sources," *Physical Review A*, vol. 98, no. 5, pp. 1–12, 2018.

[83] S. Pezzagna and J. Meijer, "Quantum computer based on color centers in diamond," *Applied Physics Reviews*, vol. 8, no. 1, 2021.

[84] R. K. Yadav, W. Liu, R. Li, T. W. Odom, G. S. Agarwal, and J. K. Basu, "Room-Temperature Coupling of Single Photon Emitting Quantum Dots to Localized and Delocalized Modes in a Plasmonic Nanocavity Array," *ACS Photonics*, vol. 8, no. 2, pp. 576–584, 2021.

[85] A. Ortu, A. Holzäpfel, J. Etesse, and M. Afzelius, "Storage of photonic time-bin qubits for up to 20 ms in a rare-earth doped crystal," pp. 1–7, 2021.

[86] M. Ghosh Dastidar, I. Thekkooden, P. K. Nayak, and V. P. Bhallamudi, "Quantum Emitters and Detectors based on 2D van der Waals Materials," *Nanoscale*, pp. 5289–5313, 2022.

[87] B. H. Lucas Novotny, *Principle of Nano-Optics*. 2012.

[88] M. Fox, *Optical Properties of Solids*. 2010.

[89] M. L. Goldman, M. W. Doherty, A. Sipahigil, N. Y. Yao, S. D. Bennett, N. B. Manson, A. Kubanek, and M. D. Lukin, "State-selective intersystem crossing in nitrogen-vacancy centers," *Physical Review B - Condensed Matter and Materials Physics*, vol. 91, no. 16, pp. 1–11, 2015.

[90] J. Friedrich and D. Haarer, "Photochemical Hole Burning: A Spectroscopic Study of Relaxation Processes in Polymers and Glasses," *Angewandte Chemie International Edition in English*, vol. 23, no. 2, pp. 113–140, 1984.

[91] T. T. Tran, C. Bradac, A. S. Solntsev, M. Toth, and I. Aharonovich, "Suppression of spectral diffusion by anti-Stokes excitation of quantum emitters in hexagonal boron nitride," *Applied Physics Letters*, vol. 115, no. 7, 2019.

[92] M. J. Holmes and Y. Arakawa, "The heat is on: towards the realization of non-cryogenic photonic quantum technologies," *Materials for Quantum Technology*, vol. 1, no. 1, p. 013001, 2021.

[93] G. Cassabois, P. Valvin, and B. Gil, "Hexagonal boron nitride is an indirect bandgap semiconductor," *Nature Photonics*, vol. 10, no. 4, pp. 262–266, 2016.

[94] K. Zhang, Y. Feng, F. Wang, Z. Yang, and J. Wang, "Two dimensional hexagonal boron nitride (2D-hBN): Synthesis, properties and applications," *Journal of Materials Chemistry C*, vol. 5, no. 46, pp. 11992–12022, 2017.

[95] X. Song, J. Gao, Y. Nie, T. Gao, J. Sun, D. Ma, Q. Li, Y. Chen, C. Jin, A. Bachmatiuk, M. H. Rümmeli, F. Ding, Y. Zhang, and Z. Liu, "Chemical vapor deposition growth of large-scale hexagonal boron nitride with controllable orientation," *Nano Research*, vol. 8, no. 10, pp. 3164–3176, 2015.

[96] C. R. Dean, A. F. Young, I. Meric, C. Lee, L. Wang, S. Sorgenfrei, K. Watanabe, T. Taniguchi, P. Kim, K. L. Shepard, and J. Hone, "Boron nitride substrates for high-quality graphene electronics," *Nature Nanotechnology*, vol. 5, no. 10, pp. 722–726, 2010.

[97] S. Roy, X. Zhang, A. B. Puthirath, A. Meiyazhagan, S. Bhattacharyya, M. M. Rahman, G. Babu, S. Susarla, S. K. Saju, M. K. Tran, L. M. Sassi, M. A. Saadi, J. Lai, O. Sahin, S. M. Sajadi, B. Dharmarajan, D. Salpekar, N. Chakingal, A. Baburaj, X. Shuai, A. Adumbumkulath, K. A. Miller, J. M. Gayle, A. Ajnsztajn, T. Prasankumar, V. V. J. Harikrishnan, V. Ojha, H. Kannan, A. Z. Khater, Z. Zhu, S. A. Iyengar, P. A. d. S. Autreto, E. F. Oliveira, G. Gao, A. G. Birdwell, M. R. Neupane, T. G. Ivanov, J. Taha-Tijerina, R. M. Yadav, S. Arepalli, R. Vajtai, and P. M. Ajayan, "Structure, Properties and Applications of Two-Dimensional Hexagonal Boron Nitride," *Advanced Materials*, vol. 33, no. 44, pp. 1–48, 2021.

[98] R. Y. Tay, *Chemical Vapor Deposition Growth and Characterization of Two-Dimensional Hexagonal Boron Nitride*. 2018.

[99] J. Meng, D. Wang, L. Cheng, M. Gao, and X. Zhang, "Recent progress in synthesis, properties, and applications of hexagonal boron nitride-based heterostructures," *Nanotechnology*, vol. 30, no. 7, 2019.

[100] S. Thomas, K. M. Ajith, and M. C. Valsakumar, "Directional anisotropy, finite size effect and elastic properties of hexagonal boron nitride," *Journal of Physics Condensed Matter*, vol. 28, no. 29, 2016.

[101] B. Niu, L. Zhong, W. Hao, Z. Yang, X. Duan, D. Cai, P. He, D. Jia, S. Li, and Y. Zhou, "First-principles study of the anisotropic thermal expansion and thermal transport properties in h-BN," *Science China Materials*, vol. 64, no. 4, pp. 953–963, 2021.

[102] K. Watanabe, T. Taniguchi, and H. Kanda, "Direct-bandgap properties and evidence for ultraviolet lasing of hexagonal boron nitride single crystal," *Nature Materials*, vol. 3, no. 6, pp. 404–409, 2004.

[103] W. Q. Han, L. Wu, Y. Zhu, K. Watanabe, and T. Taniguchi, "Structure of chemically derived mono- and few-atomic-layer boron nitride sheets," *Applied Physics Letters*, vol. 93, no. 22, pp. 1–4, 2008.

[104] K. Watanabe and T. Taniguchi, "Hexagonal boron nitride as a new ultraviolet luminescent material and its application," *International Journal of Applied Ceramic Technology*, vol. 8, no. 5, pp. 977–989, 2011.

[105] D. Wickramaratne, L. Weston, and C. G. Van De Walle, "Monolayer to Bulk Properties of Hexagonal Boron Nitride," *Journal of Physical Chemistry C*, vol. 122, no. 44, pp. 25524–25529, 2018.

[106] C. Elias, P. Valvin, T. Pelini, A. Summerfield, C. J. Mellor, T. S. Cheng, L. Eaves, C. T. Foxon, P. H. Beton, S. V. Novikov, B. Gil, and G. Cassabois, "Direct band-gap crossover in epitaxial monolayer boron nitride," *Nature Communications*, vol. 10, no. 1, pp. 1–7, 2019.

[107] J. Zhang, R. Sun, D. Ruan, M. Zhang, Y. Li, K. Zhang, F. Cheng, Z. Wang, and Z. M. Wang, "Point defects in two-dimensional hexagonal boron nitride: A perspective," *Journal of Applied Physics*, vol. 128, no. 10, 2020.

[108] L. Britnell, R. V. Gorbachev, R. Jalil, B. D. Belle, F. Schedin, M. I. Katsnelson, L. Eaves, S. V. Morozov, A. S. Mayorov, N. M. Peres, A. H. Castro Neto, J. Leist, A. K. Geim, L. A. Ponomarenko, and K. S. Novoselov, "Electron tunneling through ultrathin boron nitride crystalline barriers," *Nano Letters*, vol. 12, no. 3, pp. 1707–1710, 2012.

[109] H. X. Jiang and J. Y. Lin, "Hexagonal boron nitride for deep ultraviolet photonic devices," *Semiconductor Science and Technology*, vol. 29, no. 8, 2014.

[110] S. B. Song, S. Yoon, S. Y. Kim, S. Yang, S. Y. Seo, S. Cha, H. W. Jeong, K. Watanabe, T. Taniguchi, G. H. Lee, J. S. Kim, M. H. Jo, and J. Kim, "Deep-ultraviolet electroluminescence and photocurrent generation in graphene/hBN/graphene heterostructures," *Nature Communications*, vol. 12, no. 1, pp. 4–12, 2021.

[111] T. T. Tran, K. Bray, M. J. Ford, M. Toth, and I. Aharonovich, "Quantum emission from hexagonal boron nitride monolayers," *Nature Nanotechnology*, vol. 11, no. 1, pp. 37–41, 2016.

[112] S. Gao, H. Y. Chen, and M. Bernardi, "Radiative properties of quantum emitters in boron nitride from excited state calculations and Bayesian analysis," *npj Computational Materials*, vol. 7, no. 1, pp. 1–7, 2021.

[113] A. Sajid, J. R. Reimers, and M. J. Ford, "Defect states in hexagonal boron nitride: Assignments of observed properties and prediction of properties relevant to quantum computation," *Physical Review B*, vol. 97, no. 6, pp. 1–9, 2018.

[114] G. S. Aga, G. S. Gurmesa, Q. Zhang, P. Singh, and C. A. Geffe, "First-principles study of the electronic and optical properties of homo-doped 2D-hBN monolayer," *Computational Condensed Matter*, vol. 30, no. December 2021, p. e00628, 2022.

[115] Y. Chen and S. Y. Quek, "Photophysical Characteristics of Boron Vacancy-Derived Defect Centers in Hexagonal Boron Nitride," *Journal of Physical Chemistry C*, vol. 125, no. 39, pp. 21791–21802, 2021.

[116] T. Korona and M. Chojecki, "Exploring point defects in hexagonal boron-nitrogen monolayers," *International Journal of Quantum Chemistry*, vol. 119, no. 14, pp. 1–19, 2019.

[117] S. A. Tawfik, S. Ali, M. Fronzi, M. Kianinia, T. T. Tran, C. Stampfl, I. Aharonovich, M. Toth, and M. J. Ford, "First-principles investigation of quantum emission from hBN defects," *Nanoscale*, vol. 9, no. 36, pp. 13575–13582, 2017.

[118] N. L. McDougall, J. G. Partridge, R. J. Nicholls, S. P. Russo, and D. G. McCulloch, "Influence of point defects on the near edge structure of hexagonal boron nitride," *Physical Review B*, vol. 96, no. 14, pp. 1–9, 2017.

[119] Y. Huang, Z. Dang, X. He, and Z. Fang, "Engineering of single-photon emitters in hexagonal boron nitride [Invited]," *Chinese Optics Letters*, vol. 20, no. 3, p. 032701, 2022.

[120] Z. Shotan, H. Jayakumar, C. R. Considine, M. Mackoit, H. Fedder, J. Wrachtrup, A. Alkauskas, M. W. Doherty, V. M. Menon, and C. A. Meriles, "Photoinduced Modification of Single-Photon Emitters in Hexagonal Boron Nitride," *ACS Photonics*, vol. 3, no. 12, pp. 2490–2496, 2016.

[121] W. Lu, *Springer Series in Optical Sciences 215 Spectroscopy of Semiconductors*.

[122] J. M. Smith, *Characterisation of single defects in diamond in the development of quantum devices*. Woodhead Publishing Limited, 2014.

[123] P. Kapusta, M. Wahl, and R. Erdmann, *Advanced Photon Counting*. 2015.

[124] M. Wahl, "PicoQuant- Time-Correlated Single Photon Counting The Principle of Time-Correlated," pp. 1–14, 2017.

[125] J. C. López Carreño, E. Zubizarreta Casalengua, B. Silva, E. Del Valle, and F. P. Laussy, "Loss of antibunching," *Physical Review A*, vol. 105, no. 2, pp. 1–20, 2022.

[126] E. B. Hanlon, R. Manoharan, T. W. Koo, K. E. Shafer, J. T. Motz, M. Fitzmaurice, J. R. Kramer, I. Itzkan, R. R. Dasari, and M. S. Feld, "Prospects for in vivo Raman spectroscopy," *Physics in Medicine and Biology*, vol. 45, no. 2, 2000.

[127] A. Gottscholl, M. Kianinia, V. Soltamov, S. Orlinskii, G. Mamin, C. Bradac, C. Kasper, K. Krambrock, A. Sperlich, M. Toth, I. Aharonovich, and V. Dyakonov, "Initialization and read-out of intrinsic spin defects in a van der Waals crystal at room temperature," *Nature Materials*, vol. 19, no. 5, pp. 540–545, 2020.

[128] Z. Mu, H. Cai, D. Chen, J. Kenny, Z. Jiang, S. Ru, X. Lyu, T. S. Koh, X. Liu, I. Aharonovich, and W. Gao, "Excited-State Optically Detected Magnetic Resonance of Spin Defects in Hexagonal Boron Nitride," *Physical Review Letters*, vol. 128, no. 21, p. 216402, 2022.